

Quantum open system description of a hybrid plasmonic cavity

*Original*

Quantum open system description of a hybrid plasmonic cavity / Vallone, Marco. - In: PHYSICAL REVIEW A. - ISSN 2469-9926. - ELETTRONICO. - 113:3(2026). [10.1103/2xfb-jcgy]

*Availability:*

This version is available at: 11583/3008827 since: 2026-03-16T14:57:51Z

*Publisher:*

APS

*Published*

DOI:10.1103/2xfb-jcgy

*Terms of use:*

This article is made available under terms and conditions as specified in the corresponding bibliographic description in the repository


*Publisher copyright*

(Article begins on next page)

## Quantum open system description of a hybrid plasmonic cavity

Marco Vallone <sup>\*</sup>

*Dipartimento di Elettronica e Telecomunicazioni, Politecnico di Torino, Corso Duca degli Abruzzi 24, 10129 Torino, Italy*

 (Received 5 December 2025; revised 6 February 2026; accepted 25 February 2026; published 16 March 2026)

We present a unified quantum open system framework for lossy plasmonic cavities, treating coherent dynamics, relaxation, dephasing, and irreversible absorption on an equal footing. The Dyson equation for the cavity photon propagator in the random-phase approximation yields a complex self-energy  $\mathcal{S}(\omega)$  that accounts for both the renormalization and damping of hybrid plasmon-photon modes. It shows that increasing losses can drive a crossover from resolvable normal-mode splitting to a regime without resolved splitting, when the damping becomes comparable to or larger than the coherent hybridization scale. Tracing out the environment yields a Liouvillian for the upper polaritons (UPs) and lower polaritons (LPs) with leakage  $\Gamma = -2\text{Im}\mathcal{S}(\omega)$ , internal UP  $\leftrightarrow$  LP scattering, and dephasing. Closed-form dynamics for populations and interbranch coherence provide analytic steady-state values, line shapes, and UP-LP quench rates, valid at low polariton density and in the ultrastrong-coupling regime. The theory is directly applicable to spectra, time-domain probes, and dissipation engineering in plasmonic and nanophotonic cavities.

DOI: [10.1103/2xfb-jcgy](https://doi.org/10.1103/2xfb-jcgy)

### I. INTRODUCTION

Confinement and modulation of light in resonant cavities enable access to the regime of extreme light-matter interactions for fundamental studies and the development of highly compact nanophotonic devices. Plasmonic nanoparticles, periodically assembled as shown in Fig. 1(a), can enhance local electromagnetic fields and trigger collective electronic excitations, such as surface plasmon polaritons (SPPs), in metallic or highly doped layers of the cavity itself [1–3]. Strong coupling between SPP and electromagnetic cavity (EC) modes eventually results in their hybridization, giving rise to upper polaritons (UPs) and lower polaritons (LPs) with Hopfield-like dispersion [4], as shown in Figs. 1(b) and 1(c). Their characteristics are exploited in photonic devices for sensing, photodetection, and nanophotonic applications [5–11].

Cavity quantum electrodynamics (CQED) provides a rigorous framework for light-matter interactions in the quantum regime [12]. In the weak-coupling limit, the Jaynes-Cummings model describes coherent excitation exchange under the rotating-wave approximation (RWA) [13–15], while the quantum Rabi model [16,17] becomes essential in the ultrastrong and deep-strong-coupling regimes [18–21], which also renormalize the bare cavity response. Experimental dispersions often exhibit a blueshift of the polaritonic branches, which has been shown to arise from the dressing of the photon propagator in the cavity by a real-valued

self-energy  $\Sigma(\omega)$ , which represents SPP-SPP interactions [22,23].

A central challenge is dissipation, arising from Ohmic losses, radiative leakage, and interfacial scattering, which reduce coherence and limit accessible light-matter coupling, especially in metals. However, several material and geometric strategies now enable substantially lower plasmonic damping: among others, atomically smooth single-crystalline Au [24,25] and Ag films [26], graphene-plasmon gratings [27], Na-based nanostructures [28], plasmonic materials based on C-boron nitride monolayers [29], graphene multilayers, and metamaterial waveguides [30,31]. These examples demonstrate that underdamped plasmonic cavities are experimentally feasible, motivating a self-consistent treatment of lossy hybrid plasmon-photon dynamics.

In this work we address the hybridization between an electromagnetic cavity mode and a collective SPP mode (two bosonic degrees of freedom) in a regime where dissipation can qualitatively reshape the polaritonic spectrum. When losses are considered, the self-energy becomes complex,

$$\mathcal{S}(\omega) = \Sigma(\omega) - i\Gamma(\omega)/2, \quad (1)$$

where  $\Gamma(\omega)$  describes irreversible coupling to electronic continua [32]. Our main technical step is to retain the full complex photon self-energy  $\mathcal{S}(\omega)$  of the Dyson-resummed photon propagator and to use it to determine the complex polariton poles (frequencies and linewidths) and to fix the leakage rates  $\Gamma_k = -2\text{Im}\mathcal{S}(\omega_k)$  entering the dressed-basis Gorini-Kossakowski-Sudarshan-Lindblad (GKSL) dynamics [32–34], thereby enabling analytic driven steady-state and time-domain predictions, including Raman-driven UP-LP oscillations in the ultrastrong-coupling (USC) regime.

Compared to Ref. [23], which focused on the polaritonic frequency dispersion induced by a real self-energy that dresses the photon propagator, here we retain the full complex

<sup>\*</sup>Contact author: marco.vallone@polito.it

*Published by the American Physical Society under the terms of the Creative Commons Attribution 4.0 International license. Further distribution of this work must maintain attribution to the author(s) and the published article's title, journal citation, and DOI.*

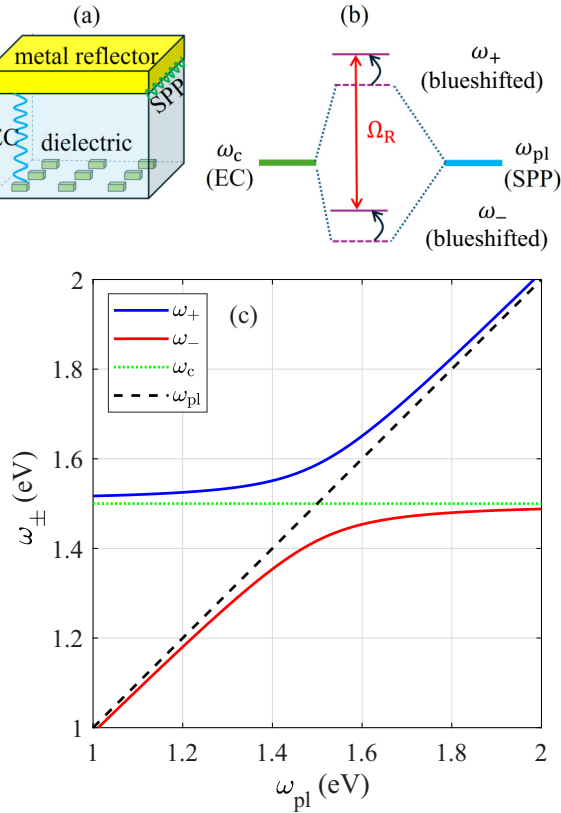


FIG. 1. (a) Sketch of a resonant plasmonic cavity illuminated at normal incidence. A lattice of gold nanoparticles on the illuminated face excites an SPP mode with frequency  $\omega_{pl}$ , set by the lattice period, that propagates along the dielectric-reflector (assumed gold) interface, while the cavity supports an EC mode at  $\omega_c$ . (b) Schematic representation of EC-SPP hybridization and (c) dispersion of eigenfrequencies  $\omega_{\pm}$  for  $\omega_c = 1.5$  eV, plasma frequency  $\Omega_{pl} \approx 8.5$  eV, dimensionless EC-SPP coupling constant  $\eta = 0.02$ , and zero losses [Eqs. (2)–(4)].

self-energy  $\mathcal{S}(\omega)$  and show that its imaginary part has qualitative consequences beyond mere linewidth broadening. In particular, the complex poles  $\omega_k$  of the dressed photon propagator determine both the polariton frequencies and their decay rates  $\Gamma_k = -2 \text{Im} \mathcal{S}(\omega_k)$ , and increasing losses can drive a crossover from resolvable normal-mode splitting to a regime without resolved splitting when the damping becomes comparable to or larger than the coherent hybridization scale.

Our approach complements existing plasmonic CQED descriptions and the general macroscopic QED quantization of absorbing media. Open system descriptions have been developed for a two-level emitter coupled to lossy single-mode SPP resonators [35], where a Green's-function formulation is recast as an effective Jaynes-Cummings model with effective emitter and resonator decay rates. Macroscopic QED and Huttner-Barnett-type models provide a fully general quantization of dispersive and absorptive environments in terms of linear response and Langevin noise operators [36,37]. Dressed-basis master equations developed for USC yield consistent reduced dynamics once the system-bath coupling operators and bath spectra are specified [38]. Here, instead of introducing independent loss rates as free parameters, we use

the microscopic self-energy  $\mathcal{S}(\omega)$ , which also determines the complex polariton poles, to fix the branch-resolved leakage rates entering the GKSL dynamics, thereby providing a direct bridge between a propagator or pole description of lossy polaritons and time-domain driven-dissipative predictions.

The structure of this work is as follows. To keep it self-contained, Sec. II reviews the Hamiltonian and Dyson propagator framework introduced in Ref. [23] to define the hybrid EC-SPP modes and their self-energy. The extension beyond Ref. [23] is the retention of the full complex self-energy and the use of its imaginary part to relate microscopic absorption to polariton linewidths. Section III formulates the GKSL reduced dynamics for UP and LP polaritons, including leakage, UP  $\leftrightarrow$  LP thermalization, and dephasing. Section IV derives closed evolution equations for coherent amplitudes, populations, and interbranch coherence, which yield analytic steady-state solutions and explain the quenching of UP-LP oscillations under coherent Raman-like driving. Section V summarizes the results and discusses open directions, such as non-Markovian effects and a microscopic noise construction consistent with fluctuation-dissipation constraints.

Throughout this work we use natural units ( $\hbar = c = k_B = 1$ , which indicate the reduced Planck constant, the light velocity in vacuum, and the Boltzmann constant, respectively) and report frequencies and energies in eV.

## II. LOSSY PLASMONIC CAVITY: HAMILTONIAN AND PROPAGATOR FORMALISMS

This section summarizes the Hamiltonian and propagator formalism used to define the hybrid EC-SPP modes and to connect them to the microscopic susceptibility of the metallic reflector. The lossless part of this derivation and the Dyson-resummed photon propagator were presented in Ref. [23]; we recall the essential steps here to keep the paper self-contained and to establish notation. The different aspect is the retention of the full complex self-energy and the use of its imaginary part to link microscopic absorption to polariton linewidths and, in Sec. III, to the GKSL open system dynamics.

We refer to the resonant plasmonic cavity sketched in Fig. 1(a) and illuminated at normal incidence by an electromagnetic field. A lattice of gold nanoparticles on the illuminated face excites an SPP mode with frequency  $\omega_{pl}$ , set by the lattice period, that propagates along the dielectric-reflector interface, while the cavity supports an EC mode at  $\omega_c$ . The reflector is assumed to be gold.

Experimentally, the nanoparticle array can function as a grating coupler: It provides the necessary in-plane momentum to access a specific SPP branch, and for a fixed illumination and collection geometry, one effectively selects a single bright Bloch mode  $k_{\parallel}$  (determined by reciprocal lattice vectors) that participates in the observed anticrossing. Near this anticrossing, the hybrid spectrum is well described by a minimal two-oscillator model (one EC mode and one collective SPP mode), while localized nanoparticle plasmons, other diffraction orders, and radiative continua mainly contribute a slowly varying background. These background contributions can be incorporated into an effective self-energy  $\mathcal{S}(\omega)$ , which may generally be structured and can reproduce non-Lorentzian or Fano line shapes [39,40]. The Drude-Lorentz form used below

is the minimal choice that preserves closed-form expressions; if necessary, more structured responses can be included by replacing  $\mathcal{S}(\omega)$  with an experimentally fitted or numerically computed function without altering the open system formulation.

There are several excellent papers in the literature that describe the EC-SPP interaction in the context of the CQED [4,41–43], in which the interaction produces hybrid modes with angular frequencies  $\omega_{\pm}$ . When modeled as an isolated system, i.e., neglecting any losses, the Hamiltonian in the Power-Zienau-Woolley multipolar picture [41,44,45] is

$$\hat{H}_s = \omega_c \left( \hat{a}^\dagger \hat{a} + \frac{1}{2} \right) + \omega_{\text{pl}} \left( \hat{b}^\dagger \hat{b} + \frac{1}{2} \right) - \frac{i\eta\Omega_{\text{pl}}}{2} (\hat{a} - \hat{a}^\dagger)(\hat{b} + \hat{b}^\dagger) + \frac{\eta^2\Omega_{\text{pl}}^2}{2} (\hat{b} + \hat{b}^\dagger)^2, \quad (2)$$

where  $\hat{a}$  and  $\hat{b}$  are bosonic annihilation operators for EC and SPP modes, respectively,  $\Omega_{\text{pl}}$  is the bulk plasma frequency, and  $\eta \in [0, 1]$  is a dimensionless EC-SPP coupling factor that depends on the cavity details. It has been demonstrated [41,46] that this formulation of  $\hat{H}_s$  is gauge invariant and equivalent to the Hopfield Hamiltonian [4]. Both include counterrotating terms and the quadratic term proportional to  $(\hat{b} + \hat{b}^\dagger)^2$ , controlled by  $\eta^2\Omega_{\text{pl}}^2$ , is the dipole-gauge counterpart of the diamagnetic  $\mathbf{A}^2$  contribution (where  $\mathbf{A}$  is the vector potential). This term produces a depolarization-induced renormalization, i.e., a blueshift of the Hamiltonian eigenfrequencies when the light-matter coupling becomes sufficiently strong.

Following Ref. [23],  $\hat{H}_s$  can be diagonalized by a Hopfield-Bogoliubov transform to obtain

$$\hat{H}_s = \sum_{k=\pm} \omega_k \hat{B}_k^\dagger \hat{B}_k = \omega_+ \hat{B}_+^\dagger \hat{B}_+ + \omega_- \hat{B}_-^\dagger \hat{B}_-, \quad (3)$$

where  $\hat{B}_{\pm}$  are bosonic annihilation operators for Fock states  $|n_{\pm}\rangle$  and the eigenvalues are

$$\omega_{\pm}^2 = \frac{\omega_c^2 + \tilde{\omega}_{\text{pl}}^2}{2} \pm \frac{\sqrt{(\omega_c^2 - \tilde{\omega}_{\text{pl}}^2)^2 + 4g^2\omega_c^2}}{2}, \quad (4)$$

with coupling strength  $g \equiv \eta \Omega_{\text{pl}}$  and  $\tilde{\omega}_{\text{pl}} \equiv \sqrt{\omega_{\text{pl}}^2 + g^2}$ . The dispersion as a function of  $\omega_{\text{pl}}$  is shown in Fig. 1(c) for  $\omega_c = 1.5$  eV,  $\Omega_{\text{pl}} \approx 8.5$  eV (typical for gold [47]), and  $\eta = 0.02$ , which yields  $g \approx 0.17$  eV. The adopted value for  $\eta$  is a representative phenomenological value, so  $g_c \equiv \eta\Omega_{\text{pl}} \approx 0.17$ – $0.18$  eV for Au with  $\Omega_{\text{pl}} \approx 8.5$ – $9$  eV. This implies a depolarization blueshift  $\tilde{\omega}_{\text{pl}} - \omega_{\text{pl}} \approx g_c^2/2\omega_{\text{pl}} \sim 10$  meV at  $\omega_{\text{pl}} = 1.5$  eV and a normalized coupling  $g_c/\omega_c \approx 0.11$ . This is consistent with experimental values in the literature for the USC regime, which report a wide range of coupling strengths that ultimately depend on the cavity details (e.g.,  $g_c/\omega_c \in [0.4, 0.6]$  in [21],  $g_c/\omega_c \sim 0.26$  in [48],  $g_c/\omega_c \sim 0.09$  in [49], and  $g_c/\omega_c \sim 0.05$  in [50]), where the quadratic contribution in the Hamiltonian and the associated blueshift are routinely required for quantitative agreement.

The energy separation between the modes  $\omega_+ - \omega_-$  has a minimum at the crossing, which can be found taking its

derivative with respect to  $\omega_{\text{pl}}$ , obtaining

$$\min(\omega_+ - \omega_-) = g, \quad (5)$$

which defines the Rabi frequency as  $\Omega_R = g$ . The coupled EC-SPP system behaves as two coupled harmonic oscillators, and  $|n_{\pm}\rangle$  are the corresponding bosonic normal modes. The description given so far is valid in the absence of losses, from the weak to the USC regimes, the latter defined as in Ref. [18], i.e., when  $\Omega_R$  approaches  $\min\{\omega_c, \omega_{\text{pl}}\}$ .

### A. Introduction of losses: Retarded propagator formalism

The spatial components of the retarded free photon propagator (Green's function)

$$D_{0,\mu\nu}^+(x-y) = \langle 0 | \mathcal{T} \hat{A}_\mu(x) \hat{A}_\nu^\dagger(y) | 0 \rangle, \quad (6)$$

where  $\mathcal{T}$  denotes the time-ordering symbol, in conjugate space are given by  $D_{0,ij}(\omega, \mathbf{k}) = \delta_{ij} \omega^2 / (\omega_{\mathbf{k}}^2 - \omega^2 + i0^+)$  [51]. The photon propagator  $D_{ij}$ , which describes the propagation of a photon in the cavity, satisfies the Dyson equation

$$D_{ij} = D_{0,ij} + D_{0,ik} \Pi^{kl} D_{lj}, \quad (7)$$

where the polarization operator  $\Pi^{kl}$  describes the interactions of EC photons with the medium.

When dominant EC and SPP modes are present,  $D_{0,ij}(\omega, \mathbf{k})$  becomes the scalar function  $D_0(\omega) = \omega^2 / (\omega_c^2 - \omega^2 + i0^+)$ . The Dyson equation then reduces to  $D = D_0 + D_0 \Pi D$ , with  $\Pi(\omega)$  proportional to the electric susceptibility of the medium  $\chi(\omega)$ , i.e.,  $\Pi(\omega) \equiv \mathcal{S}(\omega) = \eta^2 \chi(\omega)$ , valid in the long-wavelength limit of the random-phase approximation [52,53]. For  $\chi(\omega)$  we adopt the Drude-Lorentz form [1,3,54]

$$\chi(\omega) = \frac{\Omega_{\text{pl}}^2}{\omega_{\text{pl}}^2 - \omega^2 - i\gamma_{\text{D}}\omega}, \quad (8)$$

where  $\gamma_{\text{D}}$  accounts for SPP absorption, and Fig. 2(a) schematically illustrates the mechanism.

Without loss of generality, all irreversible losses or leakage is meant to come from the absorption losses in the metallic reflector, described by the imaginary part of  $\chi(\omega)$ , assuming for the gold reflector  $\gamma_{\text{D}} \approx 0.05$  eV [47]. An additional, independent leakage channel (e.g., finite mirror reflectivity, outcoupling to free space, or roughness), although not explicitly included in the present description, can be considered as well without any difficulty; for example, the radiative losses at cavity boundaries, i.e., the mirrors, can be described by introducing a factor  $-i\kappa\omega$  instead of the  $+0^+$  in the expression of the free photon propagator  $D_0(\omega)$ , where  $\kappa$  is the bare photon loss rate at mirrors.

The solution to the Dyson equation is

$$D(\omega) = \frac{1}{D_0^{-1}(\omega) - \mathcal{S}(\omega)} = \frac{\omega^2(\omega_{\text{pl}}^2 - \omega^2 - i\gamma_{\text{D}}\omega)}{(\omega_c^2 - \omega^2)(\omega_{\text{pl}}^2 - \omega^2 - i\gamma_{\text{D}}\omega) - \omega^2 g^2}. \quad (9)$$

Neglecting leakage ( $\gamma_{\text{D}} = 0$ ), the four poles of  $D(\omega)$  are the symmetric  $\pm\omega_{\pm}$ , with  $\omega_{\pm}$  given by Eq. (4),

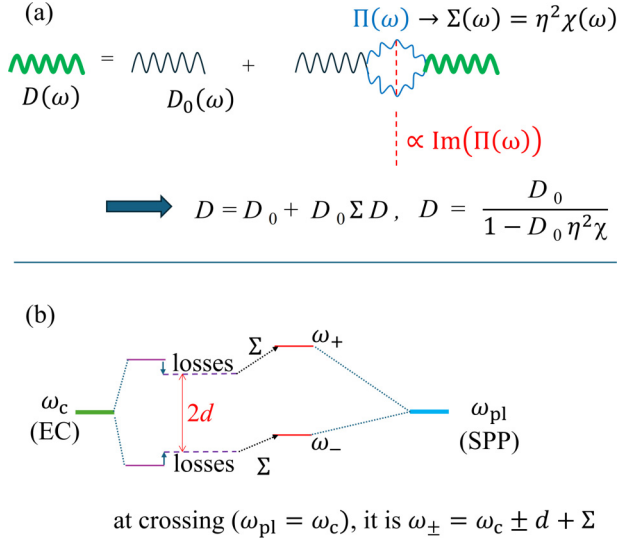


FIG. 2. (a) Diagrammatic view of the Dyson equation for  $D$ , with amplitude damping represented as the imaginary part of the self-energy. The free photon propagator  $D_0$  is dressed by the polarization bubble  $\Pi(\omega)$ . The vertical dashed cut through the bubble represents on-pole intermediate states and yields  $2 \text{Im } \mathcal{S}(\omega)$  (optical theorem in [51], Chap. 4), i.e., physical loss channels (absorption in the metal). (b) EC-SPP hybridization in the strong-coupling regime with losses, which reduce (and possibly set to zero) the Rabi frequency splitting.

confirming the equivalence of the Hamiltonian and propagator formalisms.<sup>1</sup>

### B. Effect of irreversible leakage at crossing

At the resonant condition  $\omega_{\text{pl}} = \omega_c$  (crossing), one can work from either the Hamiltonian or propagator side. However, the latter is convenient here because the impact of leakage appears directly in the denominator of Eq. (9).

To obtain the eigenfrequencies at crossing, we equate the denominator of Eq. (9) to the product  $(\omega - \omega_+)(\omega + \omega_+^*)(\omega - \omega_-)(\omega + \omega_-^*)$  and require

$$\omega_{\pm} = \omega_c \pm d + \Sigma - i\Gamma/2, \quad (10)$$

where  $d$  quantifies the mode splitting,  $\Sigma = \Re[\mathcal{S}]$  is the energy renormalization, and  $\Gamma = -2 \text{Im } \mathcal{S}$  defines the linewidth. Matching the coefficients of the characteristic polynomial yields the analytic expressions (valid at crossing)

$$d^2 = \frac{\omega_c^2}{2} + \frac{g^2}{4} - \frac{3}{32}\gamma_D^2 - \frac{1}{8}\sqrt{16\omega_c^4 - \gamma_D^2\left(2\omega_c^2 + g^2 + \frac{5}{16}\gamma_D^2\right)}, \quad (11)$$

<sup>1</sup>The four poles represent two physical modes, the LP and the UP; the positive frequencies  $\omega_{\pm}$  are the corresponding mode energies, while the two poles at  $-\omega_{\pm}$  are required by reality and causality.

$$\Sigma = -\omega_c + \frac{1}{2}\left\{2\omega_c^2 + g^2 - \frac{3}{8}\gamma_D^2 + 2\sqrt{\omega_c^4 - \frac{1}{16}[(2\omega_c^2 + g^2)\gamma_D^2 + 5\gamma_D^4]}\right\}^{1/2},$$

$$\Gamma = \gamma_D/2. \quad (12)$$

The Rabi frequency

$$\Omega_R = (\omega_+ - \omega_-)_{\omega_{\text{pl}}=\omega_c} = 2d \quad (13)$$

is set entirely by  $d$  (the common shift  $\Sigma$  cancels). In the lossless limit, we recover  $d \rightarrow g/2$  and  $\Omega_R \rightarrow g$ .

For sufficiently large losses,  $d^2$  becomes negative, signaling an exceptional point and the loss of a real normal-mode splitting, as shown in Figs. 3(a) and 3(b). The value of the loss rate  $\gamma_{D, \text{EP}}$  above which this happens is determined by the condition  $d^2 = 0$ , which yields

$$\gamma_{D, \text{EP}}^2 = \frac{1}{7}(8g^2 + 16\omega_c^2 - 4\sqrt{16\omega_c^4 - 40g^2\omega_c^2 - 10g^4}). \quad (14)$$

Figure 3(c) shows  $\gamma_{D, \text{EP}}$  as a function of  $g/\omega_c$  according to Eq. (14), with the compact estimate  $\gamma_{D, \text{EP}} \approx 2g$  valid in the experimentally relevant regime  $\{g, \gamma_D\} \ll \omega_c$ . A well-working plasmonic cavity has  $\gamma_D \ll \gamma_{D, \text{EP}}$ , since for  $\gamma_D > \gamma_{D, \text{EP}}$  the hybrid modes are distinguished by their decay rates rather than by their resonance frequencies.

Even when the influence of losses on the dispersion is small, their inclusion is essential for a consistent open system description of the plasmonic cavity. In Sec. III the full complex self-energy  $\mathcal{S}(\omega)$  is shown to enter the open system dynamics through the density operator: Although its real part  $\Sigma(\omega)$  only renormalizes the Hamiltonian and can be removed from the dynamics, its imaginary part  $-\Gamma/2$  defines the irreversible damping channel that contributes a non-Hermitian term to the Liouvillian and directly affects the dynamics. This establishes a self-consistent connection between the microscopic electron response, the Green's-function description of the cavity, and the density-matrix dynamics. Also UP  $\leftrightarrow$  LP relaxation-excitation processes (e.g., phonon-assisted ones [55,56]) are shown to determine the dynamics of the system and will be described in a similar way by means of a separate contribution to the Liouvillian of the system.

Although several expressions in this section are derived at resonance for compactness, the propagator denominator in Eq. (9) can be treated for arbitrary cavity-plasmon detuning,  $\Delta_0 \equiv \omega_c - \omega_{\text{pl}}$ . Away from resonance, the two polariton branches carry unequal EC-SPP fractions (Hopfield coefficients [41]) and their linewidths generally become asymmetric [40]. Operationally, one can first solve the pole equation given by the dressed propagator denominator in Eq. (9) (or equivalently diagonalize  $\hat{H}_s$  without imposing  $\omega_c = \omega_{\text{pl}}$ ) to obtain the complex polariton frequencies  $\omega_{\pm}(\Delta_0)$ . Then the corresponding Hopfield-Bogoliubov coefficients can be extracted, in particular, the projection of the plasmon quadrature onto each branch,

$$\hat{X}_{\text{pl}} = \sum_{k=\pm} x_k(\Delta_0)(\hat{B}_k + \hat{B}_k^\dagger) + \dots, \quad (15)$$

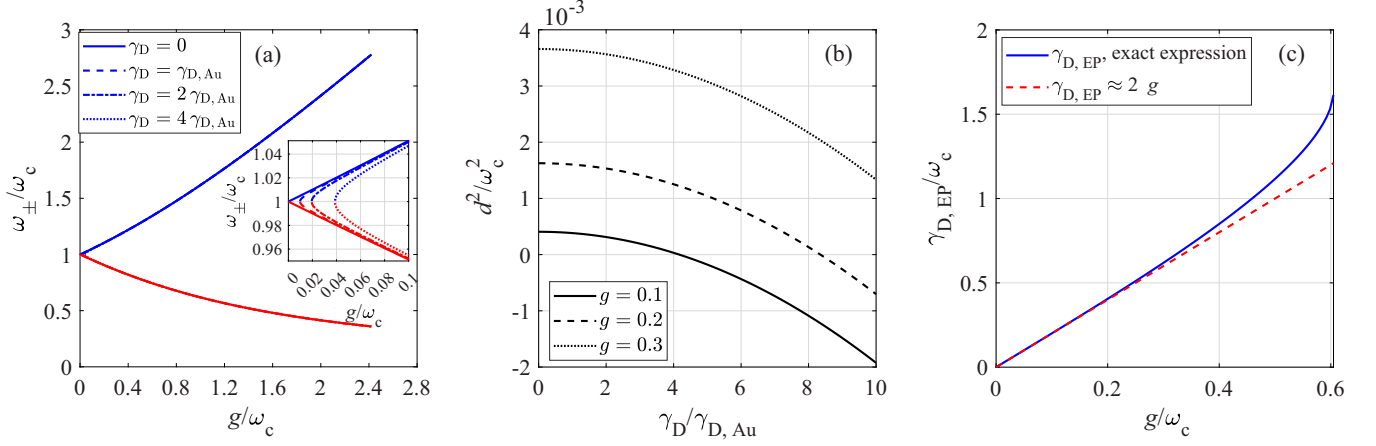


FIG. 3. (a) Eigenvalues  $\omega_{\pm}$  as a function of the normalized coupling strength  $g/\omega_c$ . The inset shows that, in the presence of losses, the polaritonic splitting does not exist for very low values of  $g/\omega_c$ . (b) Normalized square polaritonic energy separation as a function of the loss rate  $\gamma_D$  normalized to the value for gold, for three values of  $g$ . (c) Loss rate  $\gamma_{D,EP}$  that defines the exceptional point, above which the polaritonic splitting cannot exist, plotted against normalized coupling strength.

where the ellipsis denotes counterrotating contributions fixed by the same diagonalization. These weights can then be used in the dressed-basis secular GKSL construction, which yields branch-resolved leakage channels

$$\begin{aligned} \dot{\hat{\rho}} &= \sum_{k=\pm} \Gamma_k(\Delta_0) \mathcal{D}[\hat{B}_k] \hat{\rho} + \dots, \\ \Gamma_k(\Delta_0) &\propto |x_k(\Delta_0)|^2 J(\omega_k), \end{aligned} \quad (16)$$

so that the more SPP-like branch typically inherits a larger linewidth than the more EC-like one. Here,  $J(\omega)$  denotes the bath spectral density of the absorption channel evaluated at  $\omega_k$ ,  $\hat{\rho}$  is the reduced density operator, and  $\mathcal{D}[\cdot]$  is the Lindblad dissipator, with definitions given in Sec. III. In the self-energy formulation, this same asymmetry is equivalently captured by evaluating the imaginary part of the retarded self-energy at the two poles  $\Gamma_{\pm}(\Delta_0) \simeq -2\text{Im} \mathcal{S}[\omega_{\pm}(\Delta_0)]$ . The same replacement  $\Gamma \rightarrow \Gamma_{\pm}$  [and detuning-dependent drive matrix elements  $f_{\pm}(\Delta_0)$ , weighted by the corresponding photonic fractions] can also be implemented in the driven steady-state and time-domain equations of Sec. IV, leading to asymmetric spectra, unequal steady-state branch populations, and detuning-dependent damping of interbranch dynamics. Moreover, the UP-LP energy separation varies with  $\Delta_0$ , which can quantitatively affect thermal activation of the LP  $\rightarrow$  UP channel.

### III. THE CAVITY AS AN OPEN SYSTEM

When losses are zero, Eqs. (10)–(12) yield the same results as Eq. (4) at crossing. However, in the presence of irreversible cavity losses characterized by  $\gamma_D$  and restricting the description to the crossing, the propagator formulation described in Sec. II most transparently captures the system's physics. Irreversible absorption, UP  $\leftrightarrow$  LP relaxation-excitation processes [55,56], and dephasing are addresses together in this section as dissipation processes relevant for cavity dynamics, within the density operator formalism for quantum open systems [32,57].

To this end, the hybrid cavity can be conveniently described as a bosonic two-mode system in the Fock polaritonic basis  $|n_+, n_-\rangle$ ,  $n_{\pm} = 0, 1, 2, \dots$  (the vacuum corresponds to  $n_+ = n_- = 0$ ). The Fock states  $|\mathbf{n}\rangle \equiv |n_+, n_-\rangle$ , generated from the vacuum by  $B_{\pm}^{\dagger}$ , are defined as

$$|\mathbf{n}\rangle = \frac{(\hat{B}_+^{\dagger})^{n_+} (\hat{B}_-^{\dagger})^{n_-}}{\sqrt{n_+! n_-!}} |0_+, 0_-\rangle,$$

$$\hat{B}_{\pm} |\mathbf{n}\rangle = \sqrt{n_{\pm}} |\mathbf{n} - \mathbf{e}_{\pm}\rangle, \quad (17)$$

with  $\mathbf{e}_+ = (1, 0)$  and  $\mathbf{e}_- = (0, 1)$ . They belong to the Hilbert space of the isolated system, the system of interest, for which  $\{|n_+, n_-\rangle\}$  is an orthonormal basis in which  $\hat{H}_s$  is diagonal,  $\hat{H}_s = \omega_+ \hat{B}_+^{\dagger} \hat{B}_+ + \omega_- \hat{B}_-^{\dagger} \hat{B}_-$ , and has eigenvalues  $E_{n_+, n_-} = n_+ \omega_+ + n_- \omega_-$ .

Working directly in this polariton dressed basis is particularly important beyond the RWA and in the USC regime, where using bare-mode dissipators may predict spurious excitations and incorrect steady states even at zero temperature [38].

A vector state  $|\phi_k\rangle$  of the Hilbert space associated with the total system, defined as the isolated system and the environment, evolves according to the von Neumann equation  $\dot{\hat{\rho}}_{\text{T}} = -i[\hat{H}_{\text{tot}}, \hat{\rho}_{\text{T}}]$ , where  $\hat{\rho}_{\text{T}} = \sum_k |\phi_k\rangle \langle \phi_k|$  is the total density operator and  $\hat{H}_{\text{tot}} = \hat{H}_s + \hat{H}_{\text{env}} + \hat{H}_{\text{I}}$  is the total Hamiltonian. Here  $\hat{H}_{\text{env}}$  is the environment (or bath) Hamiltonian and  $\hat{H}_{\text{I}}$  describes the system-bath interactions. Tracing over the environment degrees of freedom, the reduced density operator  $\hat{\rho}$  is defined as

$$\begin{aligned} \hat{\rho} &= \sum_{\mathbf{n}, \mathbf{m}} \rho_{\mathbf{n}, \mathbf{m}} |\mathbf{n}\rangle \langle \mathbf{m}|, \\ \rho_{\mathbf{n}, \mathbf{m}} &\equiv \rho_{n_+, n_-; m_+, m_-} \\ &= \langle \mathbf{n} | \hat{\rho} | \mathbf{m} \rangle \equiv \langle n_+, n_- | \hat{\rho} | m_+, m_- \rangle, \end{aligned} \quad (18)$$

and in the Markovian approximation it evolves according to the Gorini-Kossakowski-Sudarshan-Lindblad master

equation [32–34]

$$\dot{\hat{\rho}} = -i[\hat{H}_s, \hat{\rho}] + \mathcal{L}\hat{\rho}, \quad (19)$$

where the Liouvillian  $\mathcal{L}\hat{\rho} = \sum_k \mathcal{D}_k \hat{\rho}$  is defined as the sum of dissipators

$$\mathcal{D}_{\text{leak}} \hat{\rho} = \sum_{k=\pm} \Gamma_k \left( \hat{B}_k \hat{\rho} \hat{B}_k^\dagger - \frac{1}{2} \{ \hat{B}_k^\dagger \hat{B}_k, \hat{\rho} \} \right), \quad (20)$$

$$\mathcal{D}_\downarrow \hat{\rho} = \gamma_\downarrow \left( \hat{B}_+^\dagger \hat{B}_+ \hat{\rho} \hat{B}_+^\dagger \hat{B}_- - \frac{1}{2} \{ \hat{B}_+^\dagger \hat{B}_- \hat{B}_+^\dagger \hat{B}_-, \hat{\rho} \} \right), \quad (21)$$

$$\mathcal{D}_\uparrow \hat{\rho} = \gamma_\uparrow \left( \hat{B}_+^\dagger \hat{B}_- \hat{\rho} \hat{B}_+^\dagger \hat{B}_+ - \frac{1}{2} \{ \hat{B}_+^\dagger \hat{B}_+ \hat{B}_+^\dagger \hat{B}_-, \hat{\rho} \} \right), \quad (22)$$

$$\mathcal{D}_\phi \hat{\rho} = \sum_{k=\pm} \gamma_{\phi,k} \left( \hat{N}_k \hat{\rho} \hat{N}_k - \frac{1}{2} \{ \hat{N}_k^2, \hat{\rho} \} \right), \quad (23)$$

which describe the absorption losses  $\mathcal{D}_{\text{leak}}$ , the UP  $\leftrightarrow$  LP relaxation-excitation processes  $\mathcal{D}_{\downarrow,\uparrow}$ , and dephasing  $\mathcal{D}_\phi$ , respectively. Here  $\hat{N}_k = \hat{B}_k^\dagger \hat{B}_k$ , while the rates  $\Gamma_k = -2 \text{Im} \mathcal{S}(\omega_k) \geq 0$  are fixed by the retarded self-energy  $\mathcal{S}(\omega) = \Sigma(\omega) - i\Gamma(\omega)/2$  (Sec. II); at crossing and in the Drude-Lorentz description of susceptibility  $\chi$ , one has  $\Gamma_+ = \Gamma_- = \gamma_D/2$ , denoted simply by  $\Gamma$ . Moreover, if the bath is thermal at inverse temperature  $\beta$ , the detailed balance imposes  $\gamma_\uparrow = \gamma_\downarrow \exp[-\beta(\omega_+ - \omega_-)]$ . It is recalled that the detailed balance condition applies only to the internal UP  $\leftrightarrow$  LP scattering channel, not to the combined dynamics.

The GKSL generator in Eqs. (19)–(23) is obtained by expressing the system-bath coupling in the polariton eigenbasis and applying the Born-Markov and secular approximations (see Appendix A). Although microscopic absorption couples to the plasmonic polarization (matter) operator, its projection onto the dressed modes yields branch-resolved leakage channels  $\sum_{k=\pm} \Gamma_k \mathcal{D}[\hat{B}_k] \hat{\rho}$ . The key point is that the leakage rates are fixed microscopically by the retarded self-energy introduced in Sec. II, namely,  $\Gamma_k = -2 \text{Im} \mathcal{S}(\omega_k)$ , so dissipation is not introduced by postulating a non-Hermitian Hopfield Hamiltonian, but enters through a causal frequency-dependent self-energy. In the same Markovian and secular limit, this construction is fully consistent with dressed-basis USC master equations, as in Ref. [38]: In our bosonic Hopfield setting, the dressed-eigenoperator expressions reduce to independent polariton jump operators with rates  $\Gamma_k \propto |x_k|^2 J_{\text{leak}}(\omega_k)$ , which are equivalently encoded here by  $\Gamma_k = -2 \text{Im} \mathcal{S}(\omega_k)$ .

Internal UP  $\leftrightarrow$  LP thermalization is instead described by the number-conserving jump operators  $\hat{J}_\downarrow = \sqrt{\gamma_\downarrow} \hat{B}_-^\dagger \hat{B}_+$  and  $\hat{J}_\uparrow = \sqrt{\gamma_\uparrow} \hat{B}_+^\dagger \hat{B}_-$ , which yield the dissipators  $\gamma_\downarrow \mathcal{D}[\hat{B}_+^\dagger \hat{B}_+]$  and  $\gamma_\uparrow \mathcal{D}[\hat{B}_+^\dagger \hat{B}_-]$  in Eqs. (21) and (22). The resulting quartic operator structure is simply the standard anticommutator contribution  $\hat{J}^\dagger \hat{J}$  of a Lindblad dissipator; in the single-excitation (linear-response) sector, it reduces to the familiar

$$\begin{aligned} \dot{p}_{\mathbf{n}} = & \Gamma[(n_+ + 1)p_{n_+,n_-} + (n_- + 1)p_{n_+,n_+} - (n_+ + n_-)p_{\mathbf{n}}] \\ & + (n_+ + 1)n_- (\gamma_\downarrow p_{n_+,n_-,1} - \gamma_\uparrow p_{\mathbf{n}}) + n_+(n_- + 1) (\gamma_\uparrow p_{n_+,-1,n_+} - \gamma_\downarrow p_{\mathbf{n}}). \end{aligned} \quad (24)$$

Equation (24) describes leakage of each polariton at rate  $\Gamma$  and UP  $\leftrightarrow$  LP scattering at rates  $\gamma_\downarrow$  and  $\gamma_\uparrow$ . It is understood that  $p_{n_+,n_-} = 0$  whenever an index is negative.

rate equations for incoherent transfer between UPs and LPs (Appendix A). The rates  $\gamma_{\downarrow,\uparrow}$  represent effective number-conserving scattering within the polariton manifold (e.g., phonon-assisted processes [55,56], disorder or roughness, or other low-energy environments) not captured by  $\mathcal{S}(\omega)$ ; for a thermal bath, they satisfy detailed balance  $\gamma_\uparrow = \gamma_\downarrow e^{-\beta(\omega_+ - \omega_-)}$ . Finally, while a common bath can in general induce cross-damping terms, within the Markovian and secular approximations such terms average out when  $\omega_+ - \omega_-$  is resolved, leading to the diagonal leakage dissipator in Eq. (20).

#### IV. DISSIPATIVE DYNAMICS OF POLARITON POPULATIONS AND COHERENCES

In Sec. IV A we work in the full number basis  $|n_+, n_-\rangle$ ,  $n_\pm = 0, 1, 2, \dots$  (including the vacuum), and derive exact equations of motion for the populations  $p_{\mathbf{n}} = \rho_{\mathbf{n},\mathbf{n}}$  and coherences  $\rho_{\mathbf{n},\mathbf{m}}$ ,  $\mathbf{n} \neq \mathbf{m}$ , within the GKSL Markovian approximations and the assumed structure of jump operators. Under the considered approximations, these equations are exact and preserve both the trace and positivity of the density operator.

In Sec. IV B we move to a complementary coarse-grained (mean-field) description, introducing the coherent amplitudes  $A_\pm = \langle B_\pm \rangle$ , the branch populations  $n_\pm = \langle \hat{N}_\pm \rangle$ , and the inter-branch coherence  $C = \langle \hat{B}_+^\dagger \hat{B}_- \rangle$ . In this description, the GKSL generator reduces to a closed set of nonlinear equations for  $(A_\pm, n_\pm, C)$ .

To clarify the developed formalism for use in experimental contexts aimed at characterizing absorption, UP-LP scattering, and dephasing rates, we calculate the time evolution of populations and coherences under a coherent continuous-wave (cw) drive with complex amplitude  $f_\pm$  at the cavity frequency  $\omega_c$ , which populates the hybrid modes  $|n_\pm\rangle$ .

In addition, we consider the subsequent application of a cw low-frequency drive at a frequency  $\omega_{\text{ext}} \approx \omega_+ - \omega_-$  with effective Raman-like coupling strength  $\Delta$  (since we set  $\hbar = 1$ ,  $f_\pm$  and  $\Delta$  have the dimensions of a rate). This approach enables exploration, as well as experimental measurement, for example, by pump-probe experiments, of the rates  $\Gamma$ ,  $\gamma_{\uparrow,\downarrow}$ , and  $\gamma_{\phi,\pm}$ . Importantly, the polariton-basis GKSL formulation disentangles leakage determined by the retarded self-energy from internal thermalization and pure dephasing channels, whereas a phenomenological linewidth alone cannot uniquely separate these mechanisms.

##### A. Population and coherence dynamics

Using the GKSL master equation, one obtains the equation for the evolution of populations (details of the derivation are given in Appendixes B and C)

The evolution of the coherences  $\rho_{\mathbf{n},\mathbf{m}}$  ( $\mathbf{n} \neq \mathbf{m}$ ) follows from the same GKSL equation as

$$\begin{aligned} \dot{\rho}_{\mathbf{n},\mathbf{m}} = & -i(E_{\mathbf{n}} - E_{\mathbf{m}}) \rho_{\mathbf{n},\mathbf{m}} \\ & + \Gamma \left[ \sqrt{(n_+ + 1)(m_+ + 1)} \rho_{n_+,n_-;m_+,m_-} - \frac{1}{2}(n_+ + m_+) \rho_{\mathbf{n},\mathbf{m}} \right] \\ & + \Gamma \left[ \sqrt{(n_- + 1)(m_- + 1)} \rho_{n_+,n_-+1;m_+,m_-+1} - \frac{1}{2}(n_- + m_-) \rho_{\mathbf{n},\mathbf{m}} \right] + \gamma_{\downarrow} \left\{ \sqrt{(n_+ + 1)n_-(m_+ + 1)m_-} \rho_{n_+,n_-+1;m_+,m_-+1} \right. \\ & \left. - \frac{1}{2} \left[ n_+(n_- + 1) + m_+(m_- + 1) \right] \rho_{\mathbf{n},\mathbf{m}} \right\} + \gamma_{\uparrow} \left\{ \sqrt{n_-(n_+ + 1)m_-(m_+ + 1)} \rho_{n_+-1,n_-+1;m_+-1,m_-+1} \right. \\ & \left. - \frac{1}{2} \left[ n_-(n_+ + 1) + m_-(m_+ + 1) \right] \rho_{\mathbf{n},\mathbf{m}} \right\} - \frac{1}{2} \sum_{k=\pm} \gamma_{\phi,k} (n_k - m_k)^2 \rho_{\mathbf{n},\mathbf{m}}. \end{aligned} \quad (25)$$

Importantly, the total trace  $\text{Tr}(\hat{\rho})$  is conserved, as required by the Lindblad formalism. A proof is provided in Appendix D. Moreover, it can be seen that the dephasing rates  $\gamma_{\phi,\pm}$  do not affect the populations and appear only in the time evolution of the coherences. The structure of Eq. (25) is standard: The first line describes free rotation at the frequency  $E_{\mathbf{n}} - E_{\mathbf{m}}$ , the second and third lines describe leakage-induced damping, the fourth and fifth lines describe UP  $\leftrightarrow$  LP transitions, and the last line gives pure dephasing suppression proportional to the number mismatch  $(n_k - m_k)^2$ . In the single-excitation truncation ( $n_+ + n_- \leq 1$ ), one recovers the familiar single-polariton optical Bloch equations [12].

### B. Mean-field approximation, coherent drive, and interbranch dynamics

Throughout this section we use a linearized mean-field description in which the Lindblad jump operators are expanded to first order in the polariton occupation numbers. The dynamical equations used here correspond to a linearized, first-moment mean-field closure appropriate for the low-density regime, where occupation numbers satisfy  $\langle N_{\pm} \rangle \ll 1$  and stimulated scattering terms proportional to  $N_+ N_-$  can be neglected. This form of mean-field approximation is standard in quantum-optical treatments of weakly excited bosonic modes and does not require large populations. Making a concrete example, when calculating mean-field approximations like  $\frac{d}{dt} \langle \hat{N}_{\pm} \rangle$ , terms like  $\langle \hat{N}_+ \hat{N}_- \rangle$  arise, which could be safely approximated by  $n_+ n_-$ . Although they represent stimulated emission and their inclusion could be important, we can discard them compared to terms proportional to  $n_{\pm}$  in the low-density regime. The resulting equations for the time evolution of populations and coherences are linear in the coherent amplitudes, but can be solved for arbitrary drive strengths. Going beyond the linear-dissipation regime requires keeping the full bosonic excitation factors in the UP  $\leftrightarrow$  LP Lindblad terms, which introduces nonlinear damping, density-dependent relaxation rates, and modifies the quench rate of UP-LP oscillations. These effects naturally emerge from the jump operators and become relevant at higher excitation densities.

Equation (24) allows us to evaluate the evolution of the occupation numbers  $\langle \hat{N}_{\pm} \rangle$  according to  $\frac{d}{dt} \langle \hat{N}_{\pm} \rangle = \text{Tr}(\hat{N}_{\pm} \hat{\rho})$ . Indicating  $\langle \hat{N}_{\pm} \rangle$  with  $n_{\pm}$ , we have (details of the calculations

are given in the Appendix F)

$$\frac{d}{dt} n_{\pm} = -\Gamma n_{\pm} \pm (\gamma_{\uparrow} n_- - \gamma_{\downarrow} n_+). \quad (26)$$

Equation (26), as derived from the GKSL equation, is exact at the level of first moments for the given choice of jump operators. Only in case we wanted to go beyond the linear model, additional terms  $\pm(\gamma_{\downarrow} - \gamma_{\uparrow})n_+n_-$  would be retained in going from Eq. (24) to Eq. (26), making it nonlinear in the occupation number. Such terms can be considered stimulated emission terms: The more quanta are present in one branch, the more efficiently the other branch is fed. Consideration of these terms is beyond the scope of the present work.

At all density regimes, however, Eq. (26) leads to the irreversible decrease of the polaritonic populations as

$$\frac{d}{dt} \langle \hat{N}_+ + \hat{N}_- \rangle = \frac{d}{dt} (n_+ + n_-) = -\Gamma (n_+ + n_-), \quad (27)$$

showing that that UP  $\leftrightarrow$  LP processes conserve the total polariton number, while leakage removes quanta at a rate  $\Gamma$  per polariton.

A coherent drive with complex amplitude  $f_{\pm}$  at the bare cavity frequency  $\omega_c$  is modeled by

$$H_{\text{drive}}(t) = \sum_{k=\pm} f_k e^{-i\omega_c t} \hat{B}_k^{\dagger} + \text{H.c.}, \quad (28)$$

with H.c. standing for Hermitian conjugate, whereas another coherent drive at rate  $\Delta$  and frequency  $\omega_{\text{ext}}$  close to  $\omega_+ - \omega_-$  couples the UP and LP polaritonic branches according to

$$\hat{H}_{\text{UP-LP}}(t) = \Delta (e^{-i\omega_{\text{ext}} t} \hat{B}_+^{\dagger} \hat{B}_- + e^{i\omega_{\text{ext}} t} \hat{B}_-^{\dagger} \hat{B}_+). \quad (29)$$

Transforming to a frame rotating at  $\omega_c$  by means of a unitary operator  $\hat{U}_c(t) = e^{i\omega_c t (\hat{N}_+ + \hat{N}_-)}$  and then writing  $\hat{H}_{\text{UP-LP}}(t)$  in the interaction picture removes the fast optical phase and makes the cw drives time independent. The effective system Hamiltonian becomes

$$\begin{aligned} \hat{H}_{\text{eff}} = & \frac{\delta}{2} (\hat{N}_+ - \hat{N}_-) + \Delta (\hat{B}_+^{\dagger} \hat{B}_- + \hat{B}_-^{\dagger} \hat{B}_+) \\ & + \sum_{k=\pm} f_k \hat{B}_k^{\dagger} + \text{H.c.}, \end{aligned} \quad (30)$$

where  $\delta = (\omega_+ - \omega_-) - \omega_{\text{ext}}$  is the detuning of  $\omega_{\text{ext}}$  from the UP-LP frequency difference.

The dissipative dynamics is generated by the GKSL Liouvillian  $\mathcal{L}\hat{\rho}$ . Introducing the average amplitudes  $A_{\pm} = \langle \hat{B}_{\pm} \rangle$

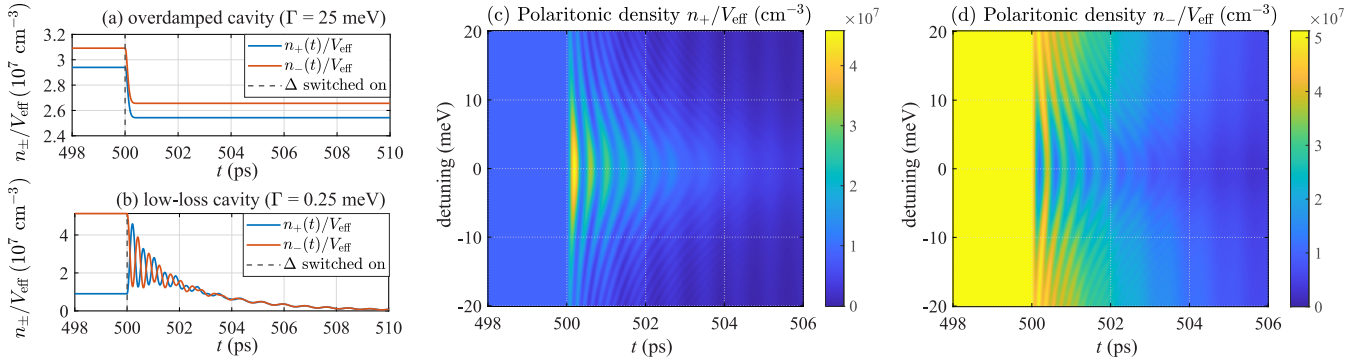


FIG. 4. (a) Time evolution of the polaritonic population densities  $n_{\pm}(t)/V_{\text{eff}}$  for the plasmonic cavity with a gold reflector (overdamped regime,  $\Gamma = \gamma_{\text{D,Au}}/2 = 25 \text{ meV}$ , lifetime approximately equal to  $0.026 \text{ ps}$ ). Because  $\Gamma \gg \Delta$ , turning on the UP-LP coherent coupling at  $t = 500 \text{ ps}$  with zero detuning ( $\delta = 0$ ) does not generate oscillatory exchange between the branches: Each mode behaves as an independently driven, strongly damped oscillator. (b) Same as in (a) but for a low-loss cavity ( $\Gamma = 0.25 \text{ meV}$ , lifetime approximately equal to  $2.6 \text{ ps}$ ), for which  $\Delta \gg \Gamma$  and long-lived relaxation oscillations appear with period  $P \approx \pi/\Delta \simeq 0.4 \text{ ps}$ . Also shown are two-dimensional color maps of (c)  $n_+(t)/V_{\text{eff}}$  and (d)  $n_-(t)/V_{\text{eff}}$  for the low-loss cavity as a function of time and detuning  $\delta$ , displaying the characteristic Lorentzian profile predicted by Eq. (36). For all simulations,  $\Delta = 5 \text{ meV}$  (approximately equal to  $7.6 \text{ ps}^{-1}$ ) is turned on at  $t = 500 \text{ ps}$ , the UP $\rightarrow$ LP relaxation rate is  $\gamma_{\downarrow} = 1 \text{ ps}^{-1}$ ,  $T = 300 \text{ K}$ , and  $\omega_+ - \omega_- = 0.1 \text{ eV}$  (yielding  $\gamma_{\uparrow} = 0.019 \text{ ps}^{-1}$ ). The population density has been evaluated for a  $(30 \times 30)\text{-}\mu\text{m}^2$  and  $1\text{-}\mu\text{m}$ -thick cavity (effective volume  $V_{\text{eff}} = 9 \times 10^{-10} \text{ cm}^3$ , just as an example).

and using  $\frac{d}{dt}\langle\hat{B}_{\pm}\rangle = \text{Tr}(\hat{B}_{\pm}\dot{\hat{\rho}})$  and the dissipators, the equations for the average amplitudes  $A_{\pm}$  are

$$\frac{d}{dt}A_+ = -\left(\frac{\Gamma + \gamma_{\phi,+}}{2} + i\frac{\delta}{2}\right)A_+ - i\Delta A_- - if_+, \quad (31)$$

$$\frac{d}{dt}A_- = -\left(\frac{\Gamma + \gamma_{\phi,-}}{2} - i\frac{\delta}{2}\right)A_- - i\Delta A_+ - if_-. \quad (32)$$

By following a similar approach, the average of the interbranch coherence  $C = \langle\hat{B}_+^{\dagger}\hat{B}_-\rangle$  is

$$\begin{aligned} \frac{d}{dt}C = & -\left(i\delta + \Gamma + \frac{\gamma_{\downarrow} + \gamma_{\uparrow}}{2} + \frac{\gamma_{\phi,+} + \gamma_{\phi,-}}{2}\right)C \\ & + i\Delta(n_- - n_+). \end{aligned} \quad (33)$$

The population equations follow from  $\dot{n}_{\pm} = \langle\hat{B}_{\pm}^{\dagger}\dot{B}_{\pm} + \dot{B}_{\pm}^{\dagger}\hat{B}_{\pm}\rangle$ , which, exploiting Eqs. (31)–(33), follow as

$$\begin{aligned} \frac{d}{dt}n_{\pm} = & -\Gamma n_{\pm} \pm (\gamma_{\uparrow}n_- - \gamma_{\downarrow}n_+) \\ & \pm 2\Delta \text{Im} C - 2 \text{Im}(f_{\pm}^*A_{\pm}). \end{aligned} \quad (34)$$

Equation (34) reduces exactly to Eq. (26) when  $\Delta = 0$  and  $f_{\pm} = 0$ .

To illustrate the dynamics governed by the dissipation rates, we solved the coupled equations (31)–(34) considering two representative cases: (a) the cavity described in Fig. 1, which resulted in overdamping due to high losses in the metal, with  $\Gamma = \gamma_{\text{D,Au}}/2 \approx 25 \text{ meV}$ , and (b) a low-loss cavity, with  $\Gamma = 0.25 \text{ meV}$ . In both cases, we set a UP $\rightarrow$ LP relaxation rate  $\gamma_{\downarrow} = 1 \text{ ps}^{-1}$  and, to avoid additional free parameters,  $\gamma_{\phi,\pm} = 0$ . The rate  $\gamma_{\uparrow}$  was evaluated from  $\gamma_{\downarrow}$  for temperature  $T = 300 \text{ K}$  and for  $\omega_+ - \omega_- = 0.1 \text{ eV}$ , which yield  $\gamma_{\uparrow} = 0.019 \text{ ps}^{-1}$ . The coherent drive at  $\omega_c$  with equal amplitudes is turned on at  $t = 0$  and the coherent Raman-like drive with  $\Delta = 5 \text{ meV}$  (or, equivalently, approximately  $7.6 \text{ ps}^{-1}$ ) is turned on at  $t = 500 \text{ ps}$ .

Figures 4(a) and 4(b) illustrate the dynamical response of the driven cavity when the coherent Raman-like UP-LP coupling  $\Delta$  is switched on at  $t = 500 \text{ ps}$  for zero detuning  $\delta = 0$ . In the overdamped case [Fig. 4(a)], the condition  $\Gamma \gg \Delta$  suppresses the effects of coherent interbranch exchange: Each branch behaves as a quasi-independently driven lossy oscillator and no oscillatory dynamics is observed after the coupling is activated.

In contrast, the low-loss cavity in Fig. 4(b) operates in the underdamped regime  $\Delta \gg \Gamma, \gamma_{\downarrow}, \gamma_{\uparrow}$ . When  $\Delta$  is switched on, the modes  $|n_{\pm}\rangle$  hybridize into new normal modes, which display pronounced relaxation oscillations with period  $P \approx \pi/\Delta \approx 0.4 \text{ ps}$ , in agreement with the Rabi-like coupling induced by the low-frequency drive. The oscillation envelope decays over a few picoseconds, consistent with the effective quench rate  $\Gamma_{\text{osc}} = \Gamma + \frac{3}{4}(\gamma_{\downarrow} + \gamma_{\uparrow})$ , which combines irreversible leakage with UP $\leftrightarrow$ LP scattering. In fact, in the linear regime and at resonant interbranch driving ( $\delta = 0$ ), the coupled dynamics of the UP-LP population difference  $\langle n_+ - n_- \rangle$  and the interbranch coherence follow a two-dimensional Bloch-type equation. Its eigenvalues are

$$\lambda_{\pm} = -\left(\Gamma + \frac{3}{4}(\gamma_{\downarrow} + \gamma_{\uparrow})\right) \pm i\sqrt{4\Delta^2 - \frac{(\gamma_{\downarrow} + \gamma_{\uparrow})^2}{16}}, \quad (35)$$

so in the underdamped regime  $\Delta > (\gamma_{\downarrow} + \gamma_{\uparrow})/8$  the UP-LP oscillations decay with an effective rate  $\Gamma_{\text{osc}} = \Gamma + \frac{3}{4}(\gamma_{\downarrow} + \gamma_{\uparrow})$ .

The coherent interbranch coupling  $\Delta$  does not introduce additional irreversible loss: The decay rate of the oscillations is determined by the real part of Eq. (35),  $\Gamma_{\text{osc}} = \Gamma + \frac{3}{4}(\gamma_{\downarrow} + \gamma_{\uparrow})$ , while  $\Delta$  controls the coherent normal-mode splitting (dressing) of the UP and LP, with oscillation frequency  $\Omega_{\text{osc}} = \sqrt{4\Delta^2 - \frac{(\gamma_{\downarrow} + \gamma_{\uparrow})^2}{16}} \approx 2\Delta$  for  $\Delta \gg \gamma_{\downarrow} + \gamma_{\uparrow}$ . Depending on the spectral resolution, this dressing may appear as an Autler-Townes-like splitting or as an increased effective width of the response envelope as a function of the interbranch-

drive detuning  $\delta$ . Consequently, the intracavity steady-state population is suppressed by a factor  $\Gamma^2/(\Gamma^2 + 4\Delta^2)$  (if  $\delta = 0$ , for simplicity), which can exceed an order of magnitude in the regime  $\Delta \gg \Gamma$ . This result can be obtained by solving the linearized driven-dissipative dynamics in the absence of internal UP  $\leftrightarrow$  LP relaxation channels, i.e., by setting  $\gamma_{\uparrow,\downarrow} = 0$  and neglecting pure dephasing. In this limit, the two polariton branches are driven symmetrically, and the steady-state occupations satisfy  $n_+ = n_-$  when  $\Delta = 0$  and for  $f_+ = f_-$ , with a doubletlike dressed response,

$$n_{\pm}^{\text{ss}}(\delta) = |f_{\pm}|^2 \frac{(\frac{\Gamma}{2})^2 + (\frac{\delta}{2} \pm \Delta)^2}{[(\frac{\Gamma}{2})^2 + (\frac{\delta}{2})^2 + \Delta^2]^2}. \quad (36)$$

When the phenomenological UP  $\leftrightarrow$  LP rates  $\gamma_{\uparrow,\downarrow}$  are restored, the steady-state populations become unequal even at  $\delta = 0$ ,  $\Delta = 0$ , and equal driving, as Figs. 4(a) and 4(b) show, with the ratio  $n_+/n_-$  determined by the rates  $\Gamma$  and  $\gamma_{\uparrow,\downarrow}$ ,

$$n_{\pm}^{\text{ss, general}}(\delta) = \frac{|-if_{\pm}(\kappa_{\mp} \mp i\frac{\delta}{2}) - \Delta f_{\mp}|^2}{|(\kappa_+ + i\frac{\delta}{2})(\kappa_- - i\frac{\delta}{2}) + \Delta^2|^2}, \quad (37)$$

where we defined  $\kappa_+ = \Gamma/2 + \gamma_{\downarrow}$  and  $\kappa_- = \Gamma/2 + \gamma_{\uparrow}$ . The reduction observed when  $\Delta$  is turned on is a coherent effect of mode hybridization: The total population still decays only through the irreversible loss rate  $\Gamma$ , while  $\Delta$  merely redistributes the injected excitations among hybridized modes with a modified decay channel.

In the case of the low-loss cavity,  $\Delta \gg \Gamma$  and Fig. 4(b) shows long-lasting relaxation oscillations with period  $P \approx \pi/\Delta \approx 0.4$  ps, not present in Fig. 4(a), which refers to the overdamped cavity.

Figures 4(c) and 4(d) further show  $n_{\pm}(t)/V_{\text{eff}}$  for the low-loss cavity as a function of detuning  $\delta$ , revealing the expected Lorentzian response that peaks at  $\delta = 0$  and broadens according to the denominator of Eq. (37) [the population density has been evaluated for a  $(30 \times 30)\text{-}\mu\text{m}^2$  and  $1\text{-}\mu\text{m}$ -thick cavity, i.e., in an effective volume  $V_{\text{eff}} = 9 \times 10^{-10}$  cm<sup>3</sup>, just as an example]. The steady-state values  $n_{\pm}^{\text{ss}}(\delta)$  extracted from Fig. 4 quantitatively match the analytic expression (37), providing a direct means of extracting the cavity loss rate  $\Gamma$  from the linewidth of the polaritonic response. Together with an experimental measure of the relaxation oscillations lifetime  $\Gamma_{\text{osc}}^{-1}$ , also  $\gamma_{\downarrow}$  can be estimated.

As a final note, it is important to emphasize that in the considered regime the system behaves linearly, so the drive amplitudes  $f_{\pm}$  and  $\Delta$  can be large as well as the field-matter coupling strength, provided the induced polariton populations remain small. This condition is naturally satisfied in plasmonic cavities, where leakage usually prevents significant population buildup.

## V. CONCLUSION

We have presented a unified description of hybrid plasmonic cavities as quantum open systems, combining the Hopfield diagonalization of the lossless Hamiltonian with a propagator renormalization based on the Dyson equation and the Drude-Lorentz susceptibility of the metallic reflector. The resulting complex self-energy  $\mathcal{S}(\omega) = \Sigma(\omega) - i\Gamma(\omega)/2$  en-

codes both the frequency renormalization and the irreversible damping of the hybrid plasmon-photon modes, capturing the microscopic origin of material losses due to absorption in the metal. It also describes possible crossover from resolvable normal-mode splitting to a regime without resolved splitting, depending on the ratio between the damping rate and the coherent hybridization scale.

Motivated by tracing out the electromagnetic and electronic environments, we modeled the dynamics by a GKSL generator that governs the populations and coherences of the upper and lower polariton branches. The Liouvillian includes leakage through  $\Gamma = -2 \text{Im } \mathcal{S}(\omega)$ , UP  $\rightarrow$  LP and LP  $\rightarrow$  UP internal scattering channels  $\gamma_{\downarrow,\uparrow}$ , and optional pure dephasing, yielding a closed evolution equation for the average polaritonic occupations. The general solution is exact within the GKSL Markovian approximations and the assumed structure of jump operators and is fully consistent with the chosen microscopic  $\chi(\omega)$  for material losses. In a mean-field picture, we obtained a tractable set of equations for the coherent amplitudes, branch populations, and interbranch coherence, enabling an analytic treatment of steady-state properties.

In the linear regime, but allowing for arbitrary interbranch coupling, field-matter coupling, and detuning, the driven steady-state populations follow Eq. (37), which generalizes the Lorentzian response formula (36) by incorporating internal UP  $\leftrightarrow$  LP scattering and asymmetric decay rates. The quench rate of the UP-LP relaxation oscillations, observed when the Raman-like interbranch coupling is activated, is found analytically to be  $\Gamma_{\text{osc}} = \Gamma + \frac{3}{4}(\gamma_{\downarrow} + \gamma_{\uparrow})$ , a simple expression derived from the eigenvalues of the linearized two-dimensional Bloch-type dynamics. These predictions are in quantitative agreement with the time-domain simulations in Fig. 4, which distinguish overdamped and underdamped regimes depending on the relative magnitudes of  $\Gamma$ ,  $\gamma_{\downarrow,\uparrow}$ , and the coherent coupling strength.

Extending the present treatment beyond the linear-dissipation regime requires retaining the full bosonic occupation factors in the UP  $\leftrightarrow$  LP Lindblad channels. Addressing this nonlinear dissipative regime, as well as incorporating non-Markovian environments, is left for future work. In particular, we aim to formulate a time-local, completely positive master equation that preserves nonsecular interference between decay pathways, while reducing to the standard secular description when the environment spectrally resolves the polariton splitting.

Finally, while any GKSL master equation admits an equivalent Heisenberg-Langevin representation (obtained by supplementing each dissipative channel with a quantum noise operator [36,37]), deriving noise correlations that are microscopically consistent with plasmonic absorption is nontrivial. In lossy and dispersive media, the fluctuations are constrained by fluctuation-dissipation relations. Moreover, when the damping originates from a frequency-dependent self-energy  $\mathcal{S}(\omega)$ , the corresponding noise is generally colored and can induce correlated fluctuations in the polariton basis. A fully consistent construction would therefore require an explicit bath model (or a macroscopic QED quantization of noise currents) whose spectral density reproduces  $\text{Im } \mathcal{S}(\omega)$ , followed by a projection onto the UP or LP operators. For

this reason, we focused here on deterministic first-moment dynamics and leave a microscopic treatment of polaritonic noise correlations for future work.

From an experimental perspective, the analytic steady-state response and time-domain predictions enable rate-resolved characterization of hybrid plasmonic cavities: The leakage rate  $\Gamma$  can be inferred from polaritonic linewidths, while the internal scattering rates  $\gamma_{\downarrow, \uparrow}$  can be extracted from the damping of UP-LP relaxation oscillations under interbranch driving. More generally, separating leakage determined by the retarded self-energy from internal thermalization and pure dephasing channels provides a diagnostic interpretation of observed broadenings and coherence decay and predicts the crossover between underdamped and overdamped regimes that define loss-limited strong coupling.

Altogether, the framework developed here provides a minimal yet self-consistent connection between microscopic material response, Green's-function electrodynamics, and open quantum system dynamics. It offers a transparent approach to modeling dissipative polariton physics in plasmonic, excitonic, and dielectric cavities and is directly applicable to pump-probe measurements, terahertz of microwave spectroscopy of UP-LP transitions, and linewidth engineering in strongly coupled nanophotonic platforms.

#### ACKNOWLEDGMENTS

This work was supported in part by the European Union under two initiatives of the Italian National Recovery and Resilience Plan of NextGenerationEU: the partnership on Telecommunications of the Future (Grant No. PE00000001, program RESTART), and the National Centre for HPC, Big Data and Quantum Computing (Grants No. CN00000013 and No. CUPE13C22000990001).

#### DATA AVAILABILITY

The data that support the findings of this article are not publicly available upon publication because it is not technically feasible and/or the cost of preparing, depositing, and hosting the data would be prohibitive within the terms of this research project. The data are available from the authors upon reasonable request.

#### APPENDIX A: DERIVATION OF THE GKSL GENERATOR IN THE POLARITON BASIS

This Appendix provides a detailed derivation of the GKSL dissipators used in Sec. III, explicitly showing how Eqs. (20)–(23) arise from standard Born-Markov theory in the dressed polariton basis. We also clarify the connection with another dressed-basis master equation from the literature (see [38]), which addresses a similar problem.

##### 1. Leakage from material absorption

We start from the system-bath partition  $\hat{H}_{\text{tot}} = \hat{H}_s + \hat{H}_{\text{env}} + \hat{H}_I$ , where  $\hat{H}_s = \omega_+ \hat{B}_+^\dagger \hat{B}_+ + \omega_- \hat{B}_-^\dagger \hat{B}_-$  is the lossless Hopfield Hamiltonian, diagonal in the polariton operators,  $\hat{H}_{\text{env}}$  is the bosonic reservoir, and the reduced dynamics is derived in the interaction picture. Ohmic absorption in the metal is modeled

by a matter-only coupling between the plasmonic polarization quadrature and the reservoir,

$$\begin{aligned} \hat{H}_I &= \hat{X}_{\text{pl}} \otimes \hat{B}, \\ \hat{B} &= \sum_{\nu} g_{\nu} (\hat{c}_{\nu} + \hat{c}_{\nu}^{\dagger}), \quad \hat{X}_{\text{pl}} \propto \hat{b} + \hat{b}^{\dagger}, \end{aligned} \quad (\text{A1})$$

where  $\hat{b}$  is the effective collective SPP (matter) mode described in Sec. II and  $\hat{B}$  denotes the collective bath operator coupled to the system in the interaction Hamiltonian.

The key point, emphasized in Ref. [38], is that beyond the RWA and in the USC regime, the system operator that couples to the bath must be decomposed into eigenoperators of  $\hat{H}_s$  [32]. Denoting by  $\Pi(\epsilon)$  the projector onto the eigenspace of  $\hat{H}_s$  with energy  $\epsilon$ , one writes

$$\begin{aligned} \hat{X}_{\text{pl}}(t) &= \sum_{\omega>0} [\hat{A}(\omega) e^{-i\omega t} + \hat{A}^{\dagger}(\omega) e^{i\omega t}], \\ \hat{A}(\omega) &= \sum_{\epsilon' - \epsilon = \omega} \Pi(\epsilon) \hat{X}_{\text{pl}} \Pi(\epsilon'). \end{aligned} \quad (\text{A2})$$

For the two-branch bosonic Hopfield Hamiltonian,  $\hat{X}_{\text{pl}}$  connects only polariton Fock states that differ by one excitation in either branch. Equivalently, expressing  $\hat{b}$  in the polariton basis

$$\begin{aligned} \hat{b} &= \sum_{k=\pm} (u_k \hat{B}_k + v_k \hat{B}_k^{\dagger}), \\ \hat{X}_{\text{pl}} &= \sum_{k=\pm} (x_k \hat{B}_k + x_k^* \hat{B}_k^{\dagger}), \quad x_k \propto u_k + v_k, \end{aligned} \quad (\text{A3})$$

implies that the only positive Bohr frequencies carried by  $\hat{X}_{\text{pl}}(t)$  are  $\omega_+$  and  $\omega_-$ , with lowering eigenoperators

$$\hat{A}(\omega_k) = x_k \hat{B}_k \quad (k = \pm). \quad (\text{A4})$$

Inserting  $\hat{H}_I(t) = \hat{X}_{\text{pl}}(t) \hat{B}(t)$  into the Born-Markov equation [32]

$$\dot{\hat{\rho}}_I(t) = - \int_0^{\infty} d\tau \text{Tr}_{\text{env}} [\hat{H}_I(t), [\hat{H}_I(t - \tau), \hat{\rho}_I(t) \otimes \hat{\rho}_{\text{env}}]] \quad (\text{A5})$$

and using the reservoir correlations yields the standard dressed-basis GKSL form (see, e.g., Sec. 3.4 in [32]). When the secular approximation is applied, cross terms oscillating at  $\pm(\omega_+ - \omega_-)$  are dropped, as they average out when the energy separation is resolved on the bath correlation time,  $|\omega_+ - \omega_-| \gg \tau_B^{-1}$ . The leakage part of the generator then reads

$$\dot{\hat{\rho}}|_{\text{leak}} = \sum_{k=\pm} (\Gamma_k^{\downarrow} \mathcal{D}[\hat{B}_k] \hat{\rho} + \Gamma_k^{\uparrow} \mathcal{D}[\hat{B}_k^{\dagger}] \hat{\rho}), \quad (\text{A6})$$

with

$$\begin{aligned} \Gamma_k^{\downarrow} &= 2\pi |x_k|^2 J_{\text{leak}}(\omega_k) [n_{\text{th}}(\omega_k) + 1], \\ \Gamma_k^{\uparrow} &= 2\pi |x_k|^2 J_{\text{leak}}(\omega_k) n_{\text{th}}(\omega_k), \end{aligned} \quad (\text{A7})$$

where  $J_{\text{leak}}(\omega) = \sum_{\nu} |g_{\nu}|^2 \delta(\omega - \nu)$  is the bath spectral density and  $n_{\text{th}}$  is the Bose occupation distribution. In our plasmonic setting, the energies  $\omega_{\pm}$  are around the eV scale, so even at room temperature  $n_{\text{th}}(\omega_{\pm}) \simeq 0$  and  $\Gamma_k^{\uparrow}$  is negligible.

Equation (A6) reduces to

$$\hat{\rho}|_{\text{leak}} = \sum_{k=\pm} \Gamma_k \mathcal{D}[\hat{B}_k] \hat{\rho}, \quad \Gamma_k \equiv \Gamma_k^\downarrow, \quad (\text{A8})$$

which is exactly Eq. (20).

The Lindblad operators in Eq. (20) are not expressed as matter-only operators: The bath couples to  $\hat{X}_{\text{pl}}$ , but after performing the GKSL derivation in the eigenbasis of  $\hat{H}_s$ , the relevant eigenoperators are the polariton lowering operators  $\hat{B}_\pm$  multiplied by the matter weights  $x_\pm$ . Moreover, in Eq. (20) we absorb  $|x_k|^2$  into the definition of the effective rates  $\Gamma_k$ ; an equivalent representation keeps explicit factors  $x_k$  in the jump operators.

Finally, within our Green's-function formulation, the same microscopic bath information is encoded in the complex self-energy  $\mathcal{S}(\omega)$  that dresses the photon propagator. In standard second-order perturbation theory, one has  $-2 \text{Im } \mathcal{S}(\omega) = 2\pi |x(\omega)|^2 J_{\text{leak}}(\omega)$  (up to sign conventions), so evaluating at the polariton poles yields  $\Gamma_k = -2 \text{Im } \mathcal{S}(\omega_k)$ , as used in Sec. II and in Eq. (20).

## 2. Internal UP $\leftrightarrow$ LP thermalization and pure dephasing

The remaining dissipators in Eqs. (21)–(23) are not fixed by the Ohmic absorption encoded in  $\mathcal{S}(\omega)$ , because they describe low-energy inelastic processes within the polariton manifold (phonons, disorder, etc.) [55,56]. A minimal number-conserving GKSL description is obtained by coupling the interbranch operator  $\hat{B}_-^\dagger \hat{B}_+$  to an auxiliary bath peaked around the frequency difference  $\omega_+ - \omega_-$ . In more detail, within the Born-Markov and secular approximations, the interbranch incoherent process is described by the number-conserving jump operators

$$\hat{J}_\downarrow = \sqrt{\gamma_\downarrow} \hat{B}_-^\dagger \hat{B}_+, \quad \hat{J}_\uparrow = \sqrt{\gamma_\uparrow} \hat{B}_+^\dagger \hat{B}_-. \quad (\text{A9})$$

Inserting them into the standard Lindblad form  $\mathcal{D}[\hat{J}_{\downarrow,\uparrow}] \hat{\rho} = \hat{J}_{\downarrow,\uparrow} \hat{\rho} \hat{J}_{\downarrow,\uparrow}^\dagger - \frac{1}{2} \{ \hat{J}_{\downarrow,\uparrow}^\dagger \hat{J}_{\downarrow,\uparrow}, \hat{\rho} \}$ , we obtain the dissipators  $\gamma_\downarrow \mathcal{D}[\hat{B}_-^\dagger \hat{B}_+]$  and  $\gamma_\uparrow \mathcal{D}[\hat{B}_+^\dagger \hat{B}_-]$ , which are exactly Eqs. (21) and (22).

The appearance of four polariton operators in Eqs. (21) and (22) naturally arises because the interbranch jump operators are bilinear,  $J_{\downarrow,\uparrow} \propto B_\mp^\dagger B_\pm$ . The quartic terms are simply the standard anticommutator contribution of the Lindblad dissipator. When considering the single-excitation sector spanned by  $\{|1, 0\rangle, |0, 1\rangle\}$ , one has  $\hat{B}_-^\dagger \hat{B}_+ |1, 0\rangle = |0, 1\rangle$  and  $\hat{B}_+^\dagger \hat{B}_- |0, 1\rangle = 0$ ; hence  $\hat{B}_-^\dagger \hat{B}_+$  acts exactly as the transition operator  $|0, 1\rangle\langle 1, 0|$ . Therefore,  $\mathcal{D}[\hat{B}_-^\dagger \hat{B}_+]$  reduces to the standard GKSL dissipator for incoherent transfer  $|1, 0\rangle \rightarrow |0, 1\rangle$  with rate  $\gamma_\downarrow$  (and analogously for the reverse process with  $\hat{B}_+^\dagger \hat{B}_-$ ). At the level of first moments, this yields the familiar rate equations  $\dot{n}_+ = -\gamma_\downarrow n_+ + \gamma_\uparrow n_-$  and  $\dot{n}_- = \gamma_\downarrow n_+ - \gamma_\uparrow n_-$ .

Pure dephasing of each branch can be derived by coupling the number operator  $\hat{N}_k = \hat{B}_k^\dagger \hat{B}_k$  to a low-frequency noise bath. This directly produces  $\gamma_{\phi,k} \mathcal{D}[\hat{N}_k]$ , which is Eq. (23).

## 3. Relation to other approaches

Other approaches in the literature lead to other master equations suitable for describing the USC regime. As

an example, in Ref. [38] a dressed-basis GKSL master equation was derived by starting from  $\hat{H}_t = \hat{X} \otimes \hat{B}$ , decomposing  $\hat{X}$  into eigenoperators  $\hat{A}(\omega)$  as in Eq. (A2), and applying Born-Markov plus secular approximations in the eigenbasis of  $\hat{H}_s$ . The resulting Lindblad is a sum over Bohr frequencies and transition operators between dressed eigenstates, weighted by matrix elements of the coupling operator. In particular, the cited reference writes the dressed dissipator as a sum over transition operators between eigenstates.

In the present bosonic Hopfield problem, the dressed eigenstates form harmonic ladders, so grouping all transitions at fixed Bohr frequency reconstructs the ladder operators themselves, e.g.,

$$\sum_{n_k \geq 1} \sqrt{n_k} |n_k - 1\rangle\langle n_k| = \hat{B}_k, \quad (\text{A10})$$

and the corresponding contributions reduce to  $\mathcal{D}[\hat{B}_k]$  with rates that include the matter-content prefactors  $|x_k|^2$  (absorbed in  $\Gamma_k$  in Sec. III). This derivation is exactly the same construction as in [38] specialized to the bosonic Hopfield Hamiltonian, with dressed eigenstates given by the polariton Fock states  $|n_+, n_-\rangle$  and coupling operator  $\hat{X} \equiv \hat{X}_{\text{pl}}$ . Since  $\hat{X}_{\text{pl}}$  only connects  $|n_+, n_-\rangle$  to  $|n_+ - 1, n_-\rangle$  and  $|n_+, n_- - 1\rangle$ , the sum of all transition operators at Bohr frequency  $\omega_k$  reconstructs the bosonic lowering operator  $\hat{B}_k$ . This shows that Eq. (20) is the Hopfield boson specialization of the dressed master equation adopted in Ref. [38].

## APPENDIX B: OPERATOR FORM OF THE MATRIX ELEMENTS IN THE POLARITON BASIS

In this Appendix we present the explicit evaluation of some relations that allow for the evaluation of any GKSL term in closed and explicit forms, followed by the explicit derivation of the time evolution of populations (the diagonal coefficients of the density matrix).

Starting from the definitions of Fock states  $|\mathbf{n}\rangle \equiv |n_+, n_-\rangle$  generated from the vacuum according to Eq. (17) in the main text, the dyadic operator

$$\hat{P}_{\mathbf{n},\mathbf{m}} \equiv |\mathbf{n}\rangle\langle \mathbf{m}| \quad (\text{B1})$$

provides a convenient operator basis. The density operator then reads

$$\hat{\rho} = \sum_{\mathbf{n},\mathbf{m}} \rho_{\mathbf{n},\mathbf{m}} \hat{P}_{\mathbf{n},\mathbf{m}}, \quad \rho_{\mathbf{n},\mathbf{m}} = \langle \mathbf{n} | \hat{\rho} | \mathbf{m} \rangle, \quad (\text{B2})$$

which can be written equivalently according to Eq. (18). From these definitions and from the operator number  $\hat{N}_k = \hat{B}_k^\dagger \hat{B}_k$ , the following useful identities follow:

$$\hat{N}_k \hat{P}_{\mathbf{n},\mathbf{m}} = n_k \hat{P}_{\mathbf{n},\mathbf{m}}, \quad \hat{P}_{\mathbf{n},\mathbf{m}} \hat{N}_k = m_k \hat{P}_{\mathbf{n},\mathbf{m}}, \quad (\text{B3})$$

$$\hat{B}_k \hat{P}_{\mathbf{n},\mathbf{m}} = \sqrt{n_k} \hat{P}_{\mathbf{n}-\mathbf{e}_k,\mathbf{m}} \quad (\text{B4})$$

$$\hat{B}_k^\dagger \hat{P}_{\mathbf{n},\mathbf{m}} = \sqrt{n_k + 1} \hat{P}_{\mathbf{n}+\mathbf{e}_k,\mathbf{m}}, \quad (\text{B5})$$

$$\hat{P}_{\mathbf{n},\mathbf{m}} \hat{B}_k = \sqrt{m_k + 1} \hat{P}_{\mathbf{n},\mathbf{m}+\mathbf{e}_k}, \quad (\text{B6})$$

$$\hat{P}_{\mathbf{n},\mathbf{m}} \hat{B}_k^\dagger = \sqrt{m_k} \hat{P}_{\mathbf{n},\mathbf{m}-\mathbf{e}_k}. \quad (\text{B7})$$

Consequently, we have, for example,

$$\hat{B}_k \hat{P}_{\mathbf{n},\mathbf{m}} \hat{B}_k^\dagger = \sqrt{n_k m_k} \hat{P}_{\mathbf{n}-\mathbf{e}_k, \mathbf{m}-\mathbf{e}_k}, \quad (\text{B8})$$

$$\begin{aligned} \hat{B}_-^\dagger \hat{B}_+ \hat{P}_{\mathbf{n},\mathbf{m}} \hat{B}_+^\dagger \hat{B}_- &= \sqrt{n_+(n_-+1)m_+(m_-+1)} \\ &\times \hat{P}_{\mathbf{n}-\mathbf{e}_+, \mathbf{m}-\mathbf{e}_+}, \end{aligned} \quad (\text{B9})$$

$$\begin{aligned} \hat{B}_+^\dagger \hat{B}_- \hat{P}_{\mathbf{n},\mathbf{m}} \hat{B}_-^\dagger \hat{B}_+ &= \sqrt{n_-(n_++1)m_-(m_++1)} \\ &\times \hat{P}_{\mathbf{n}+\mathbf{e}_+, \mathbf{m}+\mathbf{e}_+}. \end{aligned} \quad (\text{B10})$$

These relations provide any GKSL term in closed form. For example,

$$\hat{B}_k \hat{\rho} \hat{B}_k^\dagger = \sum_{\mathbf{n},\mathbf{m}} \rho_{\mathbf{n},\mathbf{m}} \sqrt{n_k m_k} \hat{P}_{\mathbf{n}-\mathbf{e}_k, \mathbf{m}-\mathbf{e}_k}, \quad (\text{B11})$$

$$\{\hat{B}_k^\dagger \hat{B}_k, \hat{\rho}\} = \sum_{\mathbf{n},\mathbf{m}} (n_k + m_k) \rho_{\mathbf{n},\mathbf{m}} \hat{P}_{\mathbf{n},\mathbf{m}}. \quad (\text{B12})$$

Together with (B2), this reproduces the elementwise evolution equations of populations and coherences.

### APPENDIX C: EXPLICIT CALCULATIONS OF POPULATIONS

Let us consider the elements of Eq. (19) that belong to populations, i.e.,  $\hat{\rho}_{\mathbf{n},\mathbf{n}}$ . The Hamiltonian operator is diagonal in the polaritonic basis,  $\hat{H}_s = \sum_{\mathbf{p}} E_{\mathbf{p}} \hat{P}_{\mathbf{p}\mathbf{p}}$ ; hence

$$\hat{H}_s \hat{P}_{\mathbf{n}\mathbf{m}} = \sum_{\mathbf{p}} E_{\mathbf{p}} \hat{P}_{\mathbf{p}\mathbf{p}} \hat{P}_{\mathbf{n}\mathbf{m}} = \sum_{\mathbf{p}} E_{\mathbf{p}} \delta_{\mathbf{p},\mathbf{n}} \hat{P}_{\mathbf{p}\mathbf{m}} = E_{\mathbf{n}} \hat{P}_{\mathbf{n}\mathbf{m}}, \quad (\text{C1})$$

$$\hat{P}_{\mathbf{n}\mathbf{m}} \hat{H}_s = \sum_{\mathbf{p}} E_{\mathbf{p}} \hat{P}_{\mathbf{n}\mathbf{m}} \hat{P}_{\mathbf{p}\mathbf{p}} = \sum_{\mathbf{p}} E_{\mathbf{p}} \delta_{\mathbf{p},\mathbf{m}} \hat{P}_{\mathbf{n}\mathbf{p}} = E_{\mathbf{m}} \hat{P}_{\mathbf{n}\mathbf{m}}, \quad (\text{C2})$$

from which the general identity  $[\hat{H}_s, \hat{P}_{\mathbf{n}\mathbf{m}}] = (E_{\mathbf{n}} - E_{\mathbf{m}}) \hat{P}_{\mathbf{n}\mathbf{m}}$  follows. For  $\mathbf{n} = \mathbf{m}$ , it is  $[\hat{H}_s, \hat{P}_{\mathbf{n}\mathbf{n}}] = (E_{\mathbf{n}} - E_{\mathbf{n}}) \hat{P}_{\mathbf{n}\mathbf{n}} = 0$ ; therefore, the commutator  $[\hat{H}_s, \hat{\rho}]$  leaves populations  $\rho_{\mathbf{n},\mathbf{n}}$  unchanged.

More generally, for a density operator  $\hat{\rho} = \sum_{\mathbf{n},\mathbf{m}} \rho_{\mathbf{n},\mathbf{m}} \hat{P}_{\mathbf{n}\mathbf{m}}$ , the general identity is  $[\hat{H}_s, \hat{\rho}] = \sum_{\mathbf{n},\mathbf{m}} \rho_{\mathbf{n},\mathbf{m}} (E_{\mathbf{n}} - E_{\mathbf{m}}) \hat{P}_{\mathbf{n}\mathbf{m}}$ , imparting phase rotations only to coherences  $\rho_{\mathbf{n},\mathbf{m}}$ , with  $\mathbf{n} \neq \mathbf{m}$ . If  $E_{\mathbf{n}} = E_{\mathbf{m}}$  are degenerate, that coherence is also stationary under  $\hat{H}_s$ .

Concerning the dissipators, it is convenient to define the diagonal coefficients of the density matrix  $\rho_{\mathbf{n},\mathbf{n}} = \langle \mathbf{n} | \hat{\rho} | \mathbf{n} \rangle \equiv \langle n_+, n_- | \hat{\rho} | n_+, n_- \rangle$  shortly as  $p_{\mathbf{n}} \equiv p_{n_+, n_-}$ . We have, for example,

$$\begin{aligned} (\mathcal{D}_{\text{leak}} \hat{\rho})_{\mathbf{n},\mathbf{n}} &= \Gamma \sum_{k=\pm} \langle \mathbf{n} | (\hat{B}_k \hat{\rho} \hat{B}_k^\dagger - \frac{1}{2} \{\hat{B}_k^\dagger \hat{B}_k, \hat{\rho}\}) | \mathbf{n} \rangle \\ &= \Gamma \sum_{k=\pm} [(n_k + 1) p_{\mathbf{n}+\mathbf{e}_k} - n_k p_{\mathbf{n}}] \\ &= \Gamma \sum_{k=\pm} (p_{\mathbf{n}+\mathbf{e}_k} (n_k + 1) - p_{\mathbf{n}} n_k) \hat{P}_{\mathbf{n},\mathbf{n}} \\ &= \Gamma (p_{n_+, n_-} (n_+ + 1) - p_{n_+, n_-} n_+) \hat{P}_{\mathbf{n},\mathbf{n}} \\ &\quad + \Gamma (p_{n_+, n_-+1} (n_- + 1) - p_{n_+, n_-} n_-) \hat{P}_{\mathbf{n},\mathbf{n}}. \end{aligned} \quad (\text{C3})$$

Therefore, for each  $\mathbf{n}$ , this dissipator contributes with a coefficient

$$\begin{aligned} [\mathcal{D}_{\text{leak}} \hat{\rho}]_{\mathbf{n}} &= \Gamma [p_{n_+, n_-} (n_+ + 1) + p_{n_+, n_-+1} (n_- + 1) \\ &\quad - p_{n_+, n_-} (n_+ + n_-)]. \end{aligned} \quad (\text{C4})$$

The explicit expressions of the other dissipators can be obtained following a similar path.

### APPENDIX D: OPERATOR AND COMPONENT PROOFS OF TRACE PRESERVATION

Let  $\text{Tr} \hat{\rho}(t) = \sum_{n_+, n_-} p_{n_+, n_-}(t)$ , where  $p_{n_+, n_-} \equiv \rho_{(n_+, n_-), (n_+, n_-)}$  are the diagonal elements in the polariton Fock basis. Using the cyclicity of the trace and  $\text{Tr}[\hat{H}_s, \hat{\rho}] = 0$ , we find

$$\begin{aligned} \frac{d}{dt} \text{Tr} \hat{\rho} &= \sum_j \text{Tr}(\mathcal{D}[L_j] \hat{\rho}) \\ &= \sum_j \left( \text{Tr}[L_j \hat{\rho} L_j^\dagger] - \frac{1}{2} \text{Tr}[L_j^\dagger L_j \hat{\rho}] - \frac{1}{2} \text{Tr}[\hat{\rho} L_j^\dagger L_j] \right) \\ &= \sum_j \left( \text{Tr}[L_j^\dagger L_j \hat{\rho}] - \frac{1}{2} \text{Tr}[L_j^\dagger L_j \hat{\rho}] - \frac{1}{2} \text{Tr}[L_j^\dagger L_j \hat{\rho}] \right) = 0. \end{aligned} \quad (\text{D1})$$

This holds separately for each dissipator: leakage (20), relaxation or excitation (21) and (22), and dephasing (23).

### APPENDIX E: EXPLICIT CALCULATIONS OF COHERENCES

This Appendix shows the explicit derivation of Eq. (25).

(i) In Appendix B we showed that for  $\mathbf{n} \neq \mathbf{m}$  it is  $[\hat{H}_s, \hat{\rho}] = \sum_{\mathbf{n},\mathbf{m}} \rho_{\mathbf{n},\mathbf{m}} (E_{\mathbf{n}} - E_{\mathbf{m}}) \hat{P}_{\mathbf{n}\mathbf{m}} \neq 0$ ; therefore it is, explicitly,

$$-i[\hat{H}_s, \hat{\rho}] = -i[(n_+ - m_+) \omega_+ + (n_- - m_-) \omega_-] \rho_{n_+, n_-; m_+, m_-}. \quad (\text{E1})$$

(ii) The leakage (absorption losses, mainly in the metal) is described by  $L_{\pm} = \sqrt{\Gamma} B_{\pm}$ . Using  $\langle n_+, n_- | \hat{B}_+ | n_+ + 1, n_- \rangle = \sqrt{n_+ + 1}$  and  $\langle m_+ + 1, m_- | \hat{B}_+^\dagger | m_+, m_- \rangle = \sqrt{m_+ + 1}$  (and similarly for  $\hat{B}_-$ ), the related dissipator  $\mathcal{D}_{\text{leak}} \hat{\rho}$  contributes to the coherences in Eq. (19) with the term

$$\begin{aligned} \Gamma \left[ \sqrt{(n_+ + 1)(m_+ + 1)} \rho_{n_+, n_-; m_+ + 1, m_-} - \frac{1}{2} (n_+ + m_+) \right. \\ \left. \rho_{n_+, n_-; m_+, m_-} + \sqrt{(n_- + 1)(m_- + 1)} \rho_{n_+, n_- + 1; m_+, m_- + 1} \right. \\ \left. - \frac{1}{2} (n_- + m_-) \rho_{n_+, n_-; m_+, m_-} \right]. \end{aligned} \quad (\text{E2})$$

(iii) The relaxation UP  $\rightarrow$  LP is determined by  $J_{\downarrow} = \sqrt{\gamma_{\downarrow}} \hat{B}_-^\dagger \hat{B}_+$ , which acts on the Fock states according to  $\hat{B}_-^\dagger \hat{B}_+ | n_+ + 1, n_- - 1 \rangle = \sqrt{(n_+ + 1)n_-} | n_+, n_- \rangle$  and  $\langle m_+, m_- | \hat{B}_+^\dagger \hat{B}_- = \sqrt{(m_+ + 1)m_-} \langle m_+ + 1, m_- - 1 |$ . Therefore, the related dissipator  $\mathcal{D}_{\downarrow} \hat{\rho}$  contributes to

coherences in Eq. (19) with the term

$$\gamma_{\downarrow} \left\{ \sqrt{(n_+ + 1)n_-(m_+ + 1)m_-} \rho_{n_+,n_-,m_+,m_-} - \frac{1}{2} [n_+(n_- + 1) + m_+(m_- + 1)] \rho_{n_+,n_-,m_+,m_-} \right\}. \quad (\text{E3})$$

The excitation LP $\rightarrow$ UP is determined by  $J_{\uparrow} = \sqrt{\gamma_{\uparrow}} \hat{B}_{+}^{\dagger} \hat{B}_{-}$ , and a similar procedure leads to the related contribution.

(iv) The dephasing is determined by  $L_{\phi,k} = \sqrt{\gamma_{\phi,k}} \hat{N}_k$ . Since  $\hat{N}_k |n_+, n_-\rangle = n_k |n_+, n_-\rangle$ , the contribution coming from the related dissipator is

$$-\frac{1}{2} \sum_{k=\pm} \gamma_{\phi,k} (n_k - m_k)^2 \rho_{n_+,n_-,m_+,m_-}. \quad (\text{E4})$$

## APPENDIX F: DERIVATION OF THE AVERAGE POPULATION EQUATIONS

We start from the exact population equation obtained from the GKSL dissipators,

$$\begin{aligned} \dot{p}_{n_+,n_-} = & \Gamma[(n_+ + 1)p_{n_+,n_-} + (n_- + 1)p_{n_+,n_-+1} \\ & - (n_+ + n_-)p_{n_+,n_-}] \\ & + (n_+ + 1)n_-(\gamma_{\downarrow} p_{n_+,n_-} - \gamma_{\uparrow} p_{n_+,n_-}) \\ & + n_+(n_- + 1)(\gamma_{\uparrow} p_{n_+,n_-} - \gamma_{\downarrow} p_{n_+,n_-}), \end{aligned} \quad (\text{F1})$$

with the convention that  $p_{n_+,n_-} = 0$  if any index is negative. The expectation values are

$$\langle \hat{N}_{+} \rangle = \sum_{n_+,n_-} n_+ p_{n_+,n_-}, \quad \langle \hat{N}_{-} \rangle = \sum_{n_+,n_-} n_- p_{n_+,n_-}. \quad (\text{F2})$$

We compute  $\frac{d}{dt} \langle \hat{N}_{\pm} \rangle = \sum_{\mathbf{n}} n_{\pm} \dot{p}_{\mathbf{n}}$  by grouping the contributions from (i) leakage  $\Gamma$ , (ii) UP $\rightarrow$ LP relaxation  $\gamma_{\downarrow}$ , and (iii) LP $\rightarrow$ UP excitation  $\gamma_{\uparrow}$ . All manipulations follow from index-shift identities such as  $p_{n_+,n_-} \mapsto p_{m_+,m_-}$  with  $m_+ = n_+ + 1$ .

### 1. Leakage

Using only the  $\Gamma$ -proportional part of Eq. (F1),

$$\begin{aligned} \dot{p}_{n_+,n_-} |_{\Gamma} = & \Gamma[(n_+ + 1)p_{n_+,n_-} + (n_- + 1)p_{n_+,n_-+1} \\ & - (n_+ + n_-)p_{n_+,n_-}], \end{aligned} \quad (\text{F3})$$

we obtain

$$\frac{d}{dt} \langle \hat{N}_{\pm} \rangle |_{\Gamma} = \sum_{n_+,n_-} n_{\pm} \dot{p}_{n_+,n_-} |_{\Gamma} \equiv T_1 + T_2 + T_3, \quad (\text{F4})$$

where, shifting the summation indices in the inflow terms,

$$T_1 = \Gamma \sum_{n_+,n_-} n_+(n_+ + 1) p_{n_+,n_-} = \Gamma(\langle \hat{N}_{+}^2 \rangle - \langle \hat{N}_{+} \rangle), \quad (\text{F5})$$

$$T_2 = \Gamma \sum_{n_+,n_-} n_+(n_- + 1) p_{n_+,n_-+1} = \Gamma \langle \hat{N}_{+} \hat{N}_{-} \rangle, \quad (\text{F6})$$

$$T_3 = -\Gamma \sum_{n_+,n_-} n_+(n_+ + n_-) p_{n_+,n_-} = -\Gamma(\langle \hat{N}_{+}^2 \rangle + \langle \hat{N}_{+} \hat{N}_{-} \rangle). \quad (\text{F7})$$

Summing them (and corresponding terms concerning  $\langle \hat{N}_{-} \rangle$ ) gives

$$\frac{d}{dt} \langle \hat{N}_{\pm} \rangle |_{\Gamma} = -\Gamma n_{\pm}. \quad (\text{F8})$$

### 2. UP $\rightarrow$ LP relaxation and LP $\rightarrow$ UP excitation

The remaining terms in Eq. (F1),

$$\begin{aligned} \dot{p}_{n_+,n_-} |_{\downarrow,\uparrow} = & (n_+ + 1)n_-(\gamma_{\downarrow} p_{n_+,n_-} - \gamma_{\uparrow} p_{n_+,n_-}) \\ & + n_+(n_- + 1)(\gamma_{\uparrow} p_{n_+,n_-} - \gamma_{\downarrow} p_{n_+,n_-}), \end{aligned} \quad (\text{F9})$$

describe population transfer between the branches. Each of the four terms is evaluated by index shifts exactly as in the leakage case. Although higher-order correlators such as  $\langle \hat{N}_{+}^2 \hat{N}_{-} \rangle$  appear at intermediate steps, these cancel out when all inflow and outflow contributions are summed. The result is the closed linear exchange law

$$\frac{d}{dt} \langle \hat{N}_{+} \rangle |_{\downarrow,\uparrow} = -\gamma_{\downarrow} n_+ + \gamma_{\uparrow} n_-, \quad (\text{F10})$$

$$\frac{d}{dt} \langle \hat{N}_{-} \rangle |_{\downarrow,\uparrow} = -\gamma_{\uparrow} n_- + \gamma_{\downarrow} n_+. \quad (\text{F11})$$

### 3. Final result

Summing the leakage (F8) and relaxation-excitation (F10) and (F11) contributions gives the coupled equations

$$\frac{d}{dt} \langle \hat{N}_{+} \rangle = -(\Gamma + \gamma_{\downarrow}) n_+ + \gamma_{\uparrow} n_-, \quad (\text{F12})$$

$$\frac{d}{dt} \langle \hat{N}_{-} \rangle = -(\Gamma + \gamma_{\uparrow}) n_- + \gamma_{\downarrow} n_+. \quad (\text{F13})$$

Adding these equations shows that UP $\leftrightarrow$ LP transitions conserve the total polariton number, while leakage removes excitations at rate  $\Gamma$ :

$$\frac{d}{dt} \langle \hat{N}_{+} + \hat{N}_{-} \rangle = -\Gamma(n_+ + n_-). \quad (\text{F14})$$

Equations (F12) and (F13) coincide with Eq. (34) when the coherent drive and the interbranch coupling are switched off, confirming the consistency between the many-polariton and mean-field descriptions.

In the main text, when the meaning is clear, we indicated  $\langle \hat{N}_{\pm} \rangle$  more simply with  $n_{\pm}$ .

- [1] H. Raether, *Surface Plasmons on Smooth and Rough Surfaces and on Gratings*, Springer Tracts in Modern Physics, Vol. 111 (Springer, Berlin, 1988).  
 [2] E. Ozbay, Plasmonics: Merging photonics and electronics at nanoscale dimensions, *Science* **311**, 189 (2006).

- [3] S. A. Maier, *Plasmonics: Fundamentals and Applications* (Springer, New York, 2007).  
 [4] J. J. Hopfield, Theory of the contribution of excitons to the complex dielectric constant of crystals, *Phys. Rev.* **112**, 1555 (1958).

- [5] H. A. Atwater and A. Polman, Plasmonics for improved photovoltaic devices, *Nat. Mater.* **9**, 205 (2010).
- [6] P. Berini, Surface plasmon–photodetectors and their applications, *Laser Photonics Rev.* **8**, 197 (2014).
- [7] J. Anker, W. P. Hall, O. O. Lyandres, N. C. Shah, J. Zhao, and R. P. V. Duyne, Biosensing with plasmonic nanosensors, *Nat. Mater.* **7**, 442 (2008).
- [8] J. Homola, S. S. Yee, and G. Gauglitz, Surface plasmon resonance sensors: Review, *Sens. Actuat. B* **54**, 3 (1999).
- [9] K. R. Catchpole and A. Polman, Plasmonic solar cells, *Opt. Express* **16**, 21793 (2008).
- [10] A. Polman and H. Atwater, Photonic design principles for ultrahigh-efficiency photovoltaics, *Nat. Mater.* **11**, 174 (2012).
- [11] S. Sarkar and T. A. F. König, Engineering plasmonic hybridization toward advanced optical sensors, *Adv. Sens. Res.* **3**, 2300054 (2024).
- [12] C. Cohen-Tannoudji, J. Dupont-Roc, and G. Grynberg, *Atom-Photon Interactions: Basic Processes and Applications* (Wiley, New York, 1992), p. 656.
- [13] E. T. Jaynes and F. W. Cummings, Comparison of quantum and semiclassical radiation theories with application to the beam maser, *Proc. IEEE* **51**, 89 (1963).
- [14] J. Liu and Z.-Y. Li, Interaction of a two-level atom with single-mode optical field beyond the rotating wave approximation, *Opt. Express* **22**, 28671 (2014).
- [15] J. Larson and T. Mavrogordatos, *The Jaynes-Cummings Model and its Descendants: Modern Research Directions*, 2nd ed. (IOP, Bristol, 2024).
- [16] I. I. Rabi, On the process of space quantization, *Phys. Rev.* **49**, 324 (1936).
- [17] I. I. Rabi, Space quantization in a gyrating magnetic field, *Phys. Rev.* **51**, 652 (1937).
- [18] C. Ciuti, G. Bastard, and I. Carusotto, Quantum vacuum properties of the intersubband cavity polariton field, *Phys. Rev. B* **72**, 115303 (2005).
- [19] P. Forn-Díaz, L. Lamata, E. Rico, J. Kono, and E. Solano, Ultrastrong coupling regimes of light-matter interaction, *Rev. Mod. Phys.* **91**, 025005 (2019).
- [20] A. F. Kockum, A. Miranowicz, S. D. Liberato, S. Savasta, and F. Nori, Ultrastrong coupling between light and matter, *Nat. Rev. Phys.* **1**, 19 (2019).
- [21] D. G. Baranov, B. Munkhbat, E. Zhukova, A. Bisht, A. Canales, B. Rousseaux, G. Johansson, T. J. Antosiewicz, and T. Shegai, Ultrastrong coupling between nanoparticle plasmons and cavity photons at ambient conditions, *Nat. Commun.* **11**, 2715 (2020).
- [22] M. Vallone, M. Goano, and A. Tibaldi, High operating temperature HgCdTe coupled cavity plasmonic infrared photodetectors, *Opt. Express* **32**, 27536 (2024).
- [23] M. Vallone, Renormalized photon propagator in quantum electrodynamics of plasmonic cavities, *New J. Phys.* **27**, 064102 (2025).
- [24] J.-S. Huang, V. Callegari, P. Geisler, C. Brünig, J. Kern, J. C. Prangma, X. Wu, T. Feichtner, J. Ziegler, P. Weinmann, M. Kamp, A. Forchel, P. Biagioni, U. Sennhauser, and B. Hecht, Atomically flat single-crystalline gold nanostructures for plasmonic nanocircuitry, *Nat. Commun.* **1**, 150 (2010).
- [25] L. Liu, A. V. Krasavin, J. Zheng, Y. Tong, P. Wang, X. Wu, B. Hecht, C. Pan, J. Li, L. Li, X. Guo, A. V. Zayats, and L. Tong, Atomically smooth single-crystalline platform for low-loss plasmonic nanocavities, *Nano Lett.* **22**, 1786 (2022).
- [26] A. S. Baburin, A. I. Ivanov, E. S. Lotkov, O. S. Sorokina, I. A. Boginskaya, E. V. Sergeev, K. A. Buzaverov, T. G. Konstantinova, D. O. Moskalev, Z. Issabayeva, I. A. Ryzhikov, and I. A. Rodionov, Epitaxial silver films morphology and optical properties evolution over two years, *Coatings* **10**, 911 (2020).
- [27] T. Guo and C. Argyropoulos, Hybrid graphene-plasmon gratings, *J. Appl. Phys.* **134**, 050901 (2023).
- [28] A. Rawashdeh, A. Wildenborg, E. Liu, Z. Gao, D. A. Czaplewski, H. Qu, J. Y. Suh, and A. Yang, High-quality surface plasmon polaritons in large-area sodium nanostructures, *Nano Lett.* **23**, 469 (2023).
- [29] A. Ghorashi, N. Rivera, B. Shi, R. Sundararaman, E. Kaxiras, J. Joannopoulos, and M. Soljačić, Highly confined, low-loss plasmonics based on two-dimensional solid-state defect lattices, *Phys. Rev. Mater.* **8**, L011001 (2024).
- [30] C. Qin, B. Wang, H. Huang, H. Long, K. Wang, and P. Lu, Low-loss plasmonic supermodes in graphene multilayers, *Opt. Express* **22**, 25324 (2014).
- [31] A. Asadi, Design of multilayer graphene metamaterials plasmonic waveguides with ultra-low-loss mid-infrared, *Optik* **327**, 172327 (2025).
- [32] H.-P. Breuer and F. Petruccione, *The Theory of Open Quantum Systems* (Oxford University Press, Oxford, 2007).
- [33] G. Lindblad, On the generators of quantum dynamical semigroups, *Commun. Math. Phys.* **48**, 119 (1976).
- [34] V. Gorini, A. Kossakowski, and E. C. G. Sudarshan, Completely positive dynamical semigroups of  $N$ -level systems, *J. Math. Phys.* **17**, 821 (1976).
- [35] T. Hümmer, F. J. García-Vidal, L. Martín-Moreno, and D. Zueco, Weak and strong coupling regimes in plasmonic QED, *Phys. Rev. B* **87**, 115419 (2013).
- [36] B. Huttner and S. M. Barnett, Quantization of the electromagnetic field in dielectrics, *Phys. Rev. A* **46**, 4306 (1992).
- [37] S. Scheel and S. Y. Buhmann, Macroscopic quantum electrodynamics—Concepts and applications, *Acta Phys. Slovaca* **58**, 675 (2008).
- [38] F. Beaudoin, J. M. Gambetta, and A. Blais, Dissipation and ultrastrong coupling in circuit QED, *Phys. Rev. A* **84**, 043832 (2011).
- [39] S. R. K. Rodriguez, A. Abass, B. Maes, O. T. A. Janssen, G. Vecchi, and J. Gómez Rivas, Coupling bright and dark plasmonic lattice resonances, *Phys. Rev. X* **1**, 021019 (2011).
- [40] A. Canales, T. Karmstrand, D. G. Baranov, T. J. Antosiewicz, and T. O. Shegai, Polaritonic linewidth asymmetry in the strong and ultrastrong coupling regime, *Nanophotonics* **12**, 4073 (2023).
- [41] Y. Todorov and C. Sirtori, Intersubband polaritons in the electrical dipole gauge, *Phys. Rev. B* **85**, 045304 (2012).
- [42] N. S. Mueller, Y. Okamura, B. G. M. Vieira, S. Juergensen, H. Lange, E. B. Barros, F. Schulz, and S. Reich, Deep strong light-matter coupling in plasmonic nanoparticle crystals, *Nature (London)* **583**, 780 (2020).
- [43] Z. Wang, L. Li, S. Wei, X. Shi, J. Xiao, Z. Guo, W. Wang, Y. Wang, and W. Wang, Manipulating light-matter interaction into strong coupling regime for photon entanglement in plasmonic lattices, *J. Appl. Phys.* **133**, 063101 (2023).

- [44] E. A. Power and S. Zienau, On the radiative contributions to the Van der Waals force, *Nuovo Cimento* **6**, 7 (1957).
- [45] R. G. Woolley and C. A. Coulson, Molecular quantum electrodynamics, *Proc. R. Soc. London A* **321**, 557 (1971).
- [46] A. Vukics, G. Konya, and P. Domokos, The gauge-invariant Lagrangian, the Power-Zienau-Woolley picture, and the choices of field momenta in nonrelativistic quantum electrodynamics, *Sci. Rep.* **11**, 16337 (2021).
- [47] R. L. Olmon, B. Slovick, T. W. Johnson, D. Shelton, S.-H. Oh, G. D. Boreman, and M. B. Raschke, Optical dielectric function of gold, *Phys. Rev. B* **86**, 235147 (2012).
- [48] D. Yoo, F. de León-Pérez, I.-H. Lee, D. A. Mohr, M. B. Raschke, J. D. Caldwell, L. Martín-Moreno, and S. H. Oh, Ultrastrong plasmon-phonon coupling via epsilon-near-zero nanocavities, *Nat. Photon.* **15**, 125 (2021).
- [49] Z. Xi, Y. Lu, W. Yu, P. Yao, P. Wang, and H. Ming, Strong coupling between plasmonic Fabry-Pérot cavity mode and magnetic plasmon, *Opt. Lett.* **38**, 1591 (2013).
- [50] P. Törmä and W. L. Barnes, Strong coupling between surface plasmon polaritons and emitters: A review, *Rep. Prog. Phys.* **78**, 013901 (2015).
- [51] M. E. Peskin and D. V. Schroeder, *Quantum Field Theory* (CRC, Boca Raton, FL, 1995).
- [52] Z. Rukelj and V. Despoja, Estimation of the single-particle band gap and exciton binding energy in two dimensional insulators: A modified  $G_0W_0$ -BSE method approach, *New J. Phys.* **22**, 063052 (2020).
- [53] S. Hughes, C. Gustin, and F. Nori, Reconciling quantum and classical spectral theories of ultrastrong coupling: role of cavity bath coupling and gauge corrections, *Opt. Quantum* **2**, 133 (2024).
- [54] N. W. Ashcroft and N. D. Mermin, *Solid State Physics* (Saunders, Philadelphia, 1976).
- [55] A. Alexandrou, G. Bianchi, E. Péronne, B. Hallé, F. Boeuf, R. André, R. Romestain, and L. Si Dang, Stimulated scattering and its dynamics in semiconductor microcavities at 80 K under nonresonant excitation conditions, *Phys. Rev. B* **64**, 233318 (2001).
- [56] T. Virgili, D. Coles, A. M. Adawi, C. Clark, P. Michetti, S. K. Rajendran, D. Brida, D. Polli, G. Cerullo, and D. G. Lidzey, Ultrafast polariton relaxation dynamics in an organic semiconductor microcavity, *Phys. Rev. B* **83**, 245309 (2011).
- [57] D. Manzano, A short introduction to the Lindblad master equation, *AIP Adv.* **10**, 025106 (2020).